Stratigraphic modelling of the Lower/Middle Oxfordian (Upper Jurassic) outer ramp deposits from the NE Paris Basin (France).

Chloé Morales, Pierre Pellenard, Benoit Vincent, Franck Smektala, Fleur Daniau, Philippe Landrein

geosciences

MDPI

Article

Stratigraphic Modelling of the Lower/Middle Oxfordian (Upper Jurassic) Outer Ramp Deposits from the NE Paris Basin (France)

Chloé Morales [1,*], Pierre Pellenard [2], Benoit Vincent [3], Franck Smektala [1], Fleur Daniau [4] and Philippe Landrein [5]

[1] INGEN-Innovation for Geosciences, 6 Rue Bastogne, 21850 Saint-Apollinaire, France
[2] Biogéosciences UMR 6282 uB/CNRS/EPHE, Université Bourgogne Franche-Comté, 21000 Dijon, France
[3] Cambridge Carbonates Ltd., 4 the Courtyard, 707 Warwick Road, Warwick B91 3DA, UK
[4] PetroXL, 101 Rue de Sèvres, 75006 Paris, France
[5] ANDRA (French National Agency for Radioactive Waste Management), Meuse/Haute-Marne Centre, 55290 Bure, France
* Correspondence: chloe.morales@ingen-geosciences.com; Tel.: +337-66-35-53-51

Abstract: We investigate herein the lateral and vertical lithological heterogeneities of the Lower/Middle Oxfordian deposits ("Terrain à Chailles" and "Marnes des Eparges" formations) in the north-eastern Paris Basin. This new detailed stratigraphic framework documents the evolution at high resolution of an outer ramp based on regional correlations in order to constrain the evolution of petrological properties between the clayey "Argiles de la Woëvre" Formation and the more calcareous "Marnes et Calcaires à Coraux de Foug Formation. The "Argiles de la Woëvre" Formation is targeted for the deep storage of nuclear waste in north-eastern France. Nine wells are correlated over the "Zone of Interest for Further Research" (ZIRA), defined by the French agency for radioactive waste management (Andra), with a resolution of 0.5–1.0 m. The architecture and the age control of these formations have been refined, revealing that the "Terrain à Chailles" Formation is characterised by a regular slightly inclined sedimentation gently deeping in the SW direction and shows a lithological evolution from silty claystones to an increased occurrence of its calcareous content towards the top (Lower Oxfordian, uppermost *mariae* and *cordatum* ammonite zones). The above "Marnes des Eparges" Formation, characterised by claystone limestone alternations, is assigned to the Middle Oxfordian (*plicatilis* ammonite zone), deposited during a slightly enhanced subsidence phase in the SE part of the basin and documented and associated with onlaps geometries on the more proximal areas. However, this change in geometry does not affect petrological properties over ZIRA, as this is not accompanied by lithological changes. The environmental factors controlling petrological heterogeneities over ZIRA are also discussed. The stepwise increase in the carbonate content and the decrease in the detrital content towards the Lower to Middle Oxfordian deposits was likely triggered by a climate change towards drier conditions, modulated by sea level changes on a ramp morphology. A major condensation phase encompassing most of the Lower Oxfordian *cordatum* ammonite zone is also highlighted. The occurrence of a maximum regressive surface associated with gentle slope topography is a probable trigger for condensation. Changes in geometries are, however, associated with the activity of the Metz Fault, which potentially had an influence on the subsidence rates of the basin at that time.

Keywords: early–middle Oxfordian transition; sequence stratigraphy; carbonate recovery; carbonate-siliciclastic ramp; Paris Basin; paleoenvironment

Citation: Morales, C.; Pellenard, P.; Vincent, B.; Smektala, F.; Daniau, F.; Landrein, P. Stratigraphic Modelling of the Lower/Middle Oxfordian (Upper Jurassic) Outer Ramp Deposits from the NE Paris Basin (France). *Geosciences* **2022**, *12*, 375. https://doi.org/10.3390/geosciences12100375

Academic Editors: Angelos G. Maravelis and Jesus Martinez-Frias

Received: 2 August 2022
Accepted: 2 October 2022
Published: 10 October 2022

1. Introduction

During subsurface geological investigations for oil and gas exploration, deep geological storage, or geothermal studies, the sequence stratigraphic correlations and models are critical to constraining the lithological and petrophysical heterogeneities of rocks [1–3]. The Paris Basin hosts numerous industrial projects linked to georesources, including geotechnical engineering, oil exploration, gas storage, carbon capture and storage (CCS), and geothermal prospects. Consequently, numerous past and ongoing geological studies provide an

exhaustive record of subsurface sedimentological, petrophysical and geochemical data and a set of robust stratigraphic schemes for various stratigraphic intervals [4–12], including the Upper Jurassic strata [13–16].

In the north-eastern part of the Paris Basin, the Andra has settled a subsurface laboratory in order to evaluate the feasibility of storage for long-life nuclear waste with medium to high radioactivity. A "Zone of Interest for Further Research" (ZIRA) was defined as well as a "Zone of Transposition" (ZT), which delimits the best potential zone for a possible future storage site. The geological target corresponds to the Callovian-Oxfordian claystone deposits, namely the "Argiles de la Woëvre" Formation also referred to as the COx Unit in this study. The COx unit has been thoroughly studied, notably for its petrophysical and geochemical properties, including mineralogy, permeability, porosity, magnetic susceptibility, and isotopic data [17–26]. The calcareous deposits overlying the COx unit consist of neritic limestones of Middle Oxfordian age (namely the "Marnes and Calcaires à coraux de Foug, that belong to the "Mésangère" Formation) and correspond to the successive stages of growth of a rimmed carbonate shelf [13–15]. Despite generally low porosity and permeability properties, these limestone-bearing successions have equally been deeply investigated for their reservoir properties and diagenetic history. These indeed represent crucial information for the constraint of paleo- and present-day hydrological systems in the aquifer overlaying the Cox [13,27–29].

If the facies evolution, geometry and petrophysical properties of the COx claystones and of the Upper Jurassic limestones are well understood, less attention has been paid to the transitional interval that precedes the carbonate platform settlement. This interval is constituted by an alternation of claystones, bioclastic marlstones and limestones ascribed to the Lower/Middle Oxfordian age and corresponding to the Terrain à Chailles and Marnes des Eparges formations, for which sedimentological studies have rather been performed at the regional scale [13,14,20,21]. The current understanding of the vertical and lateral variability of these claystone-limestone alternations is therefore limited in the ZIRA area and mostly made at a regional scale resolution, which may lead to uncertainties for the technical design of the shafts of the future possible repository site.

This study aims to build a robust stratigraphic model of this transitional interval with the objective of obtaining a predictive view of lithological and geomechanical properties of the Terrain à Chailles and Marnes des Eparges formations in the ZT. This model brings insights into the design of sealing areas in potential forthcoming wells and descents in the ZT. Nine wells distributed over the ZT were studied, providing an exceptionally extensive record of these transitional deposits in a relatively small area (252 km^2,), and an insightful constraint to wireline log traces. Electrofacies were computed using wireline logs (Gamma Ray, Resistivity and PEF) to complete the dataset in uncored wells and intervals. Beyond the scope of recognising heterogeneities and precise geometry of these deposits at a regional scale, this new stratigraphical model is discussed in light of the factors controlling the sedimentation and the recovery of carbonates during the Late Jurassic by integrating local and allogenic parameters such as climate, paleotopography, sea level changes and tectonics.

2. Geological Setting

2.1. Geographical and Structural Context

The ZIRA is located near the town of Bure (Meuse area, NE France). The area belongs to the northeast part of the Paris Basin (Figure 1), which is an intracratonic basin bordered by Hercynian crystalline massifs formed during the Variscan orogeny [30]. The eastern edge of the basin shows a homoclinal structure slightly dipping westward towards the centre. Such geometry is linked to two main subsidence phases: the first with higher rates during the Triassic–Jurassic interval and the second with lower rates during the Cretaceous-Eocene interval [30,31]. The Paris Basin is structured by faults, some inherited from the Variscan orogeny, which were reactivated during a Mesozoic extensive tectonic phase and an Eocene transpressional tectonic phase [6,30,32–34]. In the eastern part of the basin, these are the

Vittel, Metz and Saint Martin de Bossenay faults. Other faults are linked to the propagation of Cenozoic grabbens that formed during the Alpine orogeny, such as the Gondrecourt, Joinville and Marne grabbens, which delineate the eastern, southern and western borders of the ZIRA, respectively (Figure 1) [30,33,35–37].

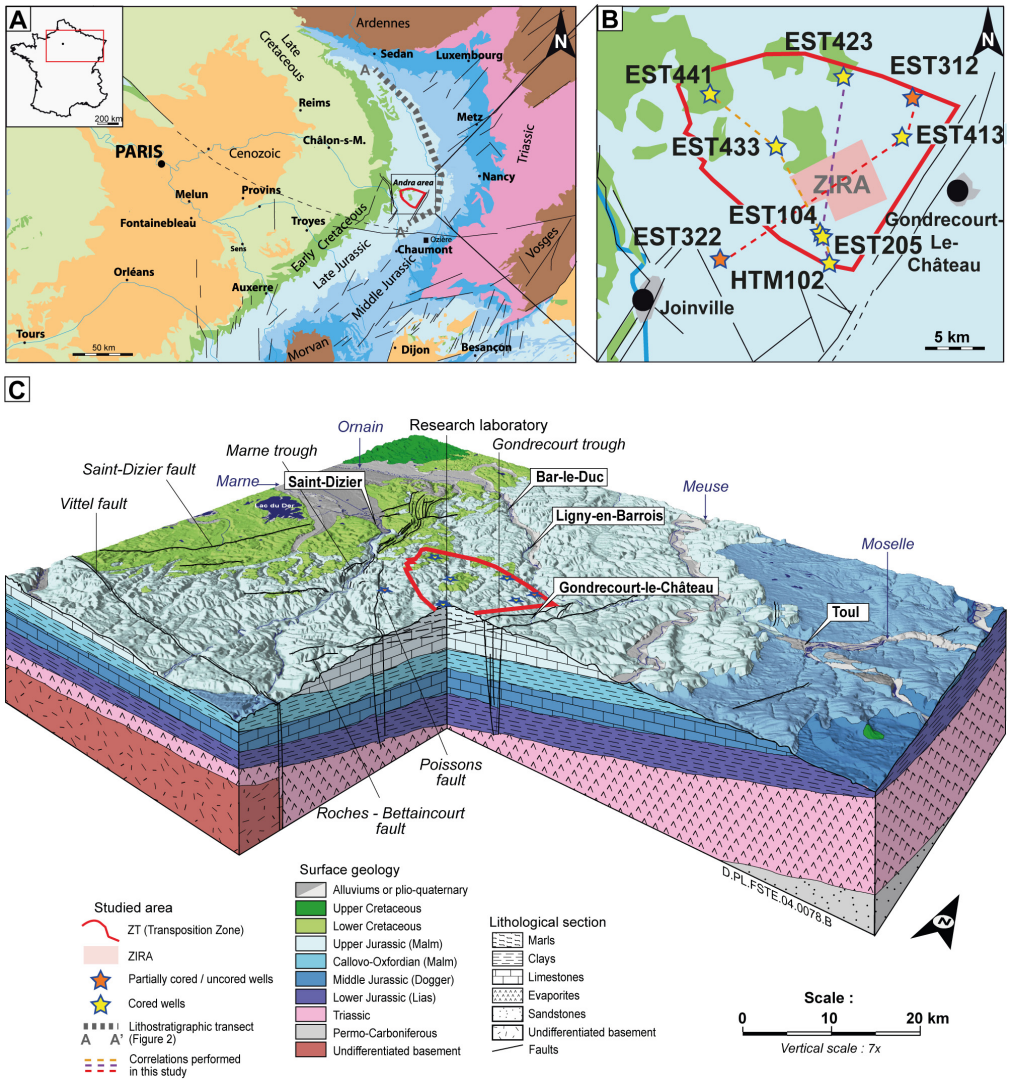

Figure 1. The studied area is located in NE France, in the northeastern part of the Paris Basin. (**A**) Geological map of the eastern part of the Paris Basin, the Zone of Transposition (ZT) is shown in red (modified after [6,30,32–34]); (**B**) Location of the ZIRA (area of interest for further research), in pink, targeted for future research, and location of the studied wells; (**C**) Geological model in 3D showing the structure of the basin.

2.2. Paleogeography and Paleoenvironments

During the Jurassic, the NW part of Europe was characterised by epicontinental seas and archipelagos between the Laurasian continent and the Tethys Ocean [38,39]. The Lorraine Platform was abutted on the London-Brabant Massif and prograded towards the southwest [9,13,40,41]. A marked change from muddy-siliciclastic towards carbonate sedimentary deposits is recorded through the Early–Middle Oxfordian boundary [13,14,40,42]. This change in sedimentation may be related to combined paleoenvironmental events, including: (i) a long-term sea-level rise [13,43,44] and (ii) a change from cool and humid to warmer and drier climate accompanied by warmer sea-water temperatures favourable to carbonate producers [20,45–48].

The increase in carbonate production during the Middle Oxfordian is also recognised in some other basins worldwide, pointing to the occurrence of a supraregional or global trigger likely related to a progressive rise in pCO_2 associated with a marine current reorganisation [49–54]. However, clumped isotope data from Russia and the oxygen isotope composition of belemnite rostra from the Polish Basin show stable values across the Oxfordian; therefore, a reorganisation of current circulations associated with a general sea-level rise is an alternative hypothesis [55–58].

2.3. Lithological and Stratigraphic Framework

The studied deposits belong to the "Terrain à Chailles" and "Marnes des Eparges" formations and are characterised by calcareous ramp deposits that overlay the outer shelf muddy clinoforms of the "Argiles de La Woëvre" Formation (COx unit) and precede the reefal systems starting from the "Marnes and Calcaires à Coraux de Foug" Formation [13,14,42] (Figure 2). Reef-bearing deposits correspond to silty calcareous shales and alternations of claystone with nodular limestones (Figure 2). In the northeast direction, the limestone beds are locally silicified [14]. The "Terrain à Chailles" Formation is dated with ammonites from the Lower Oxfordian *cordatum* Zone (upper part, after [59,60]. In the ZIRA, the "Terrain à Chailles" Formation is divided into two lithological units, named "Unité de Transition" (UT)" and the first part of the "Unité Silto-Carbonatée" (USC1), marking a change from claystone to argillaceous limestone deposits (Figure 3). The "Marnes des Eparges" Formation consists of alternations of calcareous claystone and bioclastic limestone beds rich in bivalves and brachiopods [14,20].

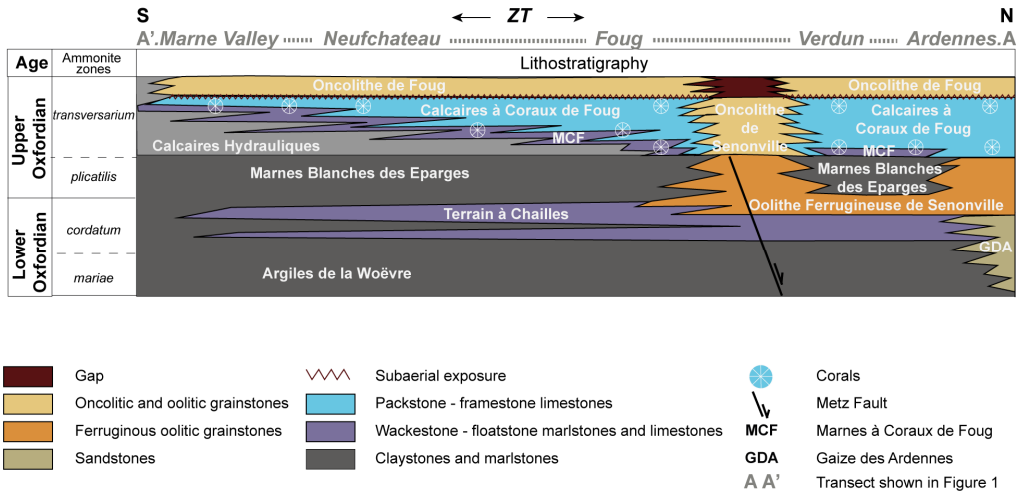

Figure 2. Lithostratigraphy of the Lower Oxfordian and lower parts of the Middle Oxfordian deposits in the NE part of the Paris Basin.

The lithological units defined by Andra in the ZIRA are grouped into the "Repère Supérieur Oolithique" unit (RSO), marked by the presence of calcareous beds and the second part of the "Unité Silto-Carbonatée" (USC2) marked by marl-limestone alternation. The latter ends with a change towards dolomicritic limestone, characterising the overlaying unit termed "Faciès Glypticien" (Figure 3). Rare ammonites sampled in USC2 give a Middle Oxfordian age, e.g., *plicatilis* zone, but the position of the Lower-Middle Oxfordian boundary remains imprecise [59]. The correlation of abentonite (altered ash layer), identified in four Andra boreholes and at Saint-Blin (a well-biostratigraphically constrained section located 20 km to the south of the ZIRA), allows the *vertebrale* subzone, *plicatilis* zone, to be precisely identified [20,21,61]. Consequently, this confirms that the USC2 unit belongs to the *plicatilis* zone, which is consistent with available ammonites from boreholes (Figure 3).

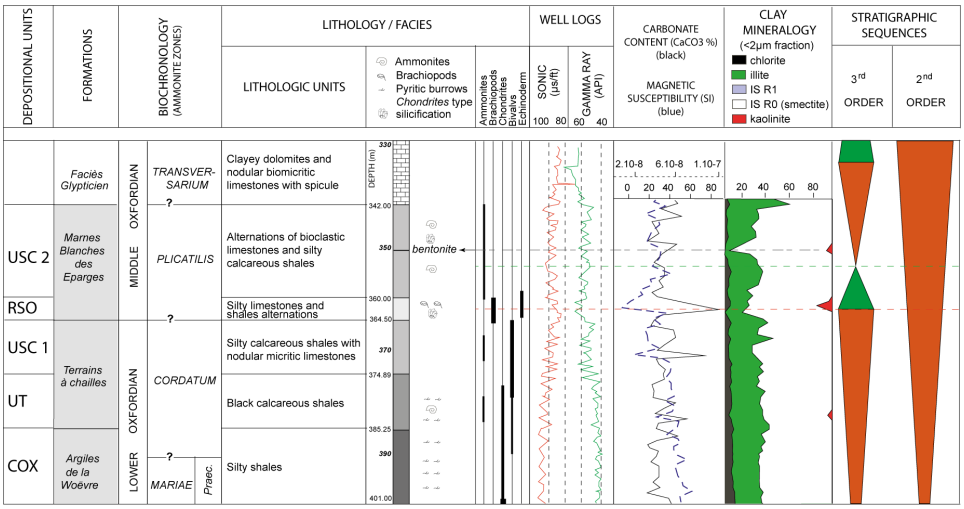

Figure 3. Lithological and sequence stratigraphic evolution of Lower and Middle Oxfordian deposits in the Bure area (adapted with permission from [13–16].

3. Materials and Methods

3.1. Sedimentological Analyses

The "Terrain à Chailles" and "Marnes des Eparges" formations were logged in eight boreholes distributed over the ZT area and around the ZIRA (EST104, EST205, EST322, EST413, EST423, EST433, EST441 and HTM102, Figure 1) at a 1:50 scale. Lithological descriptions were made following the classification scheme of [62,63], leading to the identification of 22 lithofacies, which were then grouped into 6 facies associations based on their lithology, depositional processes and faunal content (Table 1). Lithology is a central parameter used for classification because uncored intervals are characterised by electrofacies. Proportions of clay, quartz and carbonate were visually estimated during the logging. A Bioturbation Index (BI) was used to classify the density of bioturbation [64]. The identification of facies associations follows Walther's law, i.e., the vertical evolution of facies associations corresponds to their lateral evolution [65,66]. Facies were then interpreted in terms of paleo-environments [67].

3.2. Electrofacies Analyses

Electrofacies analyses were performed with the aim of completing uncored intervals in the non-cored EST312 well. The method is a statistical approach that establishes a link between two independent datasets: the core descriptions (i.e., lithofacies) and wireline logs. The computation of electrofacies is based on the definition of thresholds applied to the most conclusive traces for lithological interpretations. Seven logs were available for all wells: Caliper, Short-spacing delay time Sonic (DT), Gamma Ray (GR), Deep and shallow resistivity, Bulk Density (RHOB/RHOZ), and Photoelectric Effect (PEF). Three traces were selected: GR, PEF and Deep resistivity, based on their higher capability to discriminate core lithofacies and for their complementarity.

For instance, some wirelines show linearly correlated signals, such as GR and DT, or shallow and deep resistivity. Therefore, the tool showing the best response to hole irregularities and the best sampling resolution was selected: GR and deep resistivity. When available, spectral GR data were used in order to distinguish the uranium (organic matter, U-rich minerals) and the Potassium/Thorium signals (clays). The decomposition of the GR signal shows that there is a minor component of radioactive minerals, such as potassic feldspar or heavy minerals, in the sedimentary succession. This is consistent with bulk rock mineralogical analyses that show only traces of potassic feldspar and accessory minerals such as apatite [21,48]. Potassium and thorium curves show the same variations, which are interpreted as changes in clay content. This is fully consistent with the available mineralogical analyses performed on the core data.

Table 1. Description of lithofacies, classification into facies associations and interpretations in terms of depositional environments.

Facies Assoc.	Lithofacies	Lithological and Textural Characteristics	Faunal Assemblages and Ichnofabrics	Depositional Environements
F1	***F1***	• Claystone with horizontal laminations	• Fauna almost absent. Some *Chondrites* bioturbations are observed (BI = 1)	Basin—sedimentation by decantation in the vicinity of dysoxic environments
F2	***F2.1***	• Silty calcareous claystone with horizontal beddings or asymertical ripples	• Rare macrofauna (ammonites, belemites). Some *Chondrites* bioturbations are observed (BI = 2)	Outer ramp—low energy currents (geostrophic or storms?) in the vicinity of dysoxic environments
	F2.2	• Calcareous claystone	• Rare macrofauna (ammonites, belemites). Few calcareous debris are locally observed (small oyster shells and serpulids)	
	F2.3	• Marlstone	• Bioturbation is important (BI = 5), in particular by the ichnognera *Rhizocorallium*	
F3	***F3.1***	• Silty bioclastic marlstone	• Occurrence of small brachiopods, bivalves and serpulids. Shells are found complete or fragmented	Outer—middle ramp transition—environment under infrequent storm influence and low energy currents
	F3.2	• Calcareous bioclastic claystone with storm deposits	• Small brachiopods, bivalves and serpulids. Shells are found complete or fragmented	
	F3.3	• Bioclastic marlstone rich in crinoid plates	• Crinoid plates are abundant. Bivalves and serpulids are equally present	
F4	***F4.1***	• Calcareous marlstone rich in bivalves and/or brachiopods	• Oysters, brachiopods, and other bivalves represent most of the macrofauna. Their shells are sometimes found complete, indicating low transportation from their life environment	Middle ramp—reworked sediment from shallower middle ramp settings
	F4.2	• Marlstone with large-size bivalves	• Bivalves of 5 to 15 cm with thin shell (of *Pinna* type) and gastropods are observed, often complete, indicating low transportation from their life environment	
	F4.3	• Marlstone with calcareous nodules containing large-size bivalves	• Large calcareous nodules containing bivalves of *Pinna* type	
	F4.4	• Marlstone with other calcareous nodules	• Nodules can include brachiopods and corals, or have a mudstone texture Some micritic nodules are bioturbated, indicating that part of them are linked to depositional conditions	
F5	***F5.1***	• Bioturbated argillaceous limestone of mudstone texture	• Highly bioturbated (BI = 5). Rare shell debris	Middle ramp—low energy environment, bivalves and brachiopods in-situ, nutrient-rich waters
	F5.2	• Silty argillaceous limestone poorly bioturbated	• Rare shell debris (BI = 0)	
	F5.3	• Argillaceous limestone rich in shell debris	• Small bivalves, serpulids and brachiopods, are found broken or complete	
	F5.4	• Argillaceous limestone rich in brachiopods	• The fauna is moslty composed of brachiopods	
	F5.5	• Argillaceous limestone rich in oyster shells	• The fauna is moslty composed of oysters	
	F5.6	• Argillaceous limestone rich in bivalves	• The fauna is moslty composed of bivalves of various genera (*Ostrea*, *Pinna*, *Gryphea*, *Pectens*)	
F6	***F6.1***	• Prominant mudstone limestone poorly bioturbated	• Prominant limestone of mudstone texture, showing partial silification of the matrix (possibly linked to the dissolution of siliceous sponges)	Middle ramp—reworked sediment from shallower middle ramp settings (photic zone—less rich-nutrient waters)
	F6.2	• Nodular wackestone/floatstone limestone rich in bivalves	• Most of the fauna is composed of bivalves of *Pinna* type (i.e., 5 to 15 cm and thin shells). Brachiopods, oysters and gastropods are equally present	
	F6.3	• Nodular wackestone/floatstone limestone rich in gastropods	• Most of the fauna is composed of gastropods and bivalves	
	F6.4	• Nodular wackestone/floatstone limestone containing corals	• Brachiopods, corals, and bivalves of various genera composed the faunal assemblages	
	F6.5	• Packstone limestone rich in crinoid plates	• Flauro faunal assemblages are composed of crinoid plates and bivalves (amongst them numerous oysters).	

The PEF allows for discriminating the facies with a higher content of carbonates from those dominated by silts and clays. Finally, resistivity is used as a compaction/cementation indicator to refine the electrofacies classification. Wireline log data from the selected tools were plotted against lithofacies data in 3D cross-plots in order to visualise the values corresponding to changes in lithofacies. The selected threshold values were then applied to the set of wireline logs, dividing them into groups of electrofacies.

3.3. Well Correlation: Sequence Stratigraphy

Wells were correlated using the principles of sequence stratigraphy integrated in Catuneanu [68,69]. In the context of a distal carbonate ramp, maximum flooding surfaces (mfs) are easier to identify than relative sea-level fall unconformities. Therefore, the cycles were first identified by MFS picking. High-frequency cycles were then characterised based on the thickness and stacking patterns of facies associations and electrofacies. Each high-frequency cycle (or high-frequency sequence) corresponds to a transgression-regression cycle bounded by two flooding surfaces (fs) or regression maxima. The record and stacking patterns of high-frequency cycles depend on the ratio between the accommodation (A) and sedimentation (S) rates. High-frequency sequences are organised into sequences of lower frequency and higher rank (i.e., of lower order).

In addition, certain levels showing particular sedimentary features are identified as remarkable levels (RL) in all wells. Moreover, firmgrounds were observed on cores at different stratigraphic levels and used for correlation. Finally, recognised high-frequency sequences and associated remarkable surfaces are correlated with the help of biostratigraphic constraints provided by ammonites and brachiopods [70], as well as the occurrence of the bentonite layer identified in 4 wells.

3.4. Regional Correlations

Correlations at larger geographic and stratigraphic scales have previously been achieved [13,14]. These studies used the concept of [71] based on transgressive-regressive sequences, which are bounded by maximum regressive surfaces (MRS). This study uses the correspondence scheme of [3] and [1] to achieve the integration of high-frequency sequences in transgressive-regressive sequences, thereby delineating transgressive deposits (T), maximum flooding surfaces (MFS) and regressive deposits (R), the latter including highstand normal regressive (HNR) and lowstand normal regressive deposits (LNR).

4. Results

4.1. Lithofacies Description

The description of the cores led to the identification of 22 lithofacies, which have been grouped into six main facies associations, noted F1 to F6 from claystone to massive limestone (Table 1 and Figure 4).

The “Terrain à Chailles” and “Marnes des Eparges” formations deposits show specific lithological characteristics based on clay, carbonate and quartz contents with singular fossil and ichnofossil assemblages. Consequently, facies associations have been interpreted in terms of paleoenvironments (Figure 4). With the exception of a thin (10 cm) bentonite layer composed of almost pure smectite [21,61] (Figure 3), the most argillaceous lithofacies are found basinward and reciprocally the most calcareous lithofacies are found landward (Figures 4 and 5).

- Facies association F1 is characterised by fainted laminated claystones with high feasibility. F1 shows limited silt and carbonate content and the absence of benthic organisms. Bioturbation is limited to a few burrows of *Chondrites* type, with a bioturbation Index (BI sensu [72]; and [64]) of 1.
- Facies association F2 is composed of calcareous claystone and may display an important amount of silt-sized quartz grains in compositional mixing (sensu [73]). F2 either shows a horizontal bedding or the occurrence of asymmetrical ripples. Benthic macrofauna are rare. Few ammonites and belemnite rostra have been found (Figure 4A).

F2 groups three lithofacies: lithofacies F2.1 shows a high detrital component (28–35% of silts), and the ichnogenus *Chondrites* is regularly found (BI = 2 to 3) (Figure 4C); F2.2 contains small shell debris; lithofacies F2.3 shows higher carbonate content in the matrix (marlstones) and is thoroughly bioturbated (BI = 5), notably by the small-sized *Rhizocorallium* traces (most of specimens are less than 10 cm long), found in both subvertical and subhorizontal position.

- Facies association F3 is constituted by bioclastic marlstones, which can contain an important silt fraction. This association groups three lithofacies with distinct detrital content (F3.1) and faunal assemblages (F3.2 and F3.3). F3 shows either horizontal laminations or low angle laminations with upward curvatures, interpreted as hummocky cross stratifications (HCS). Bioclasts commonly accumulate parallel to the bedding in these facies. Lithofacies F3.1 and F3.2 contain small oyster fragments, serpulids and brachiopods. Bivalves of a large size belonging to the *Mytilidae* family have been observed in life positions. A larger diversity of carbonate producers is observed with the occurrence of crinoid plates, which can become dominant in lithofacies F3.3.
- Facies association F4 shows the occurrence of marlstones with brachiopods, bivalves (F4.1 and 4.2) and calcareous nodules (F4.3 and F4.4). Bivalves and brachiopods are not found in life positions, but their shells are often complete and relatively well preserved. Large-sized bivalves (5 to 15 cm) with thin shells (of *Pinna* type; F4.2) are increasingly shallowing upward. Bivalves and brachiopods can form nodules, characterising the lithofacies F3.6 (shells being either infilled by carbonate sediment or used as a nucleus for the precipitation of secondary carbonates, Figure 4D). Calcareous nodules are also found around massive corals, but some are purely micritic, as in lithofacies F4.4.
- Facies association F5 is characterised by argillaceous limestone and consists of a grouping of six lithofacies. Argillaceous limestone devoid of macrofauna can be either highly or poorly bioturbated (Figure 4E,F; from F5.1, with BI = 5 and F5.2, with BI = 0, respectively). They can contain small-size fragmented bioclasts (serpulids, bivalves and brachiopods in F5.3) and benthic organisms in life positions or poorly transported, such as brachiopods (F5.4), oysters (F5.5) and bivalves of various genera (*Pinna*, *Gryphea*, *Pectenids*, F5.6).
- Facies association F6 encompasses massive limestone with generally low fine clastic content (clay and silt), forming decimetre-thick stacked beds. The base and top of beds are often undulated, and beds yield a nodular aspect (Figure 4G,H). Carbonate mudstone (sensu [74]; lithofacies F6.1) is extremely stiff. Wackestone and floatstone limestones contain accumulations of benthic organisms. Lithofacies F6.2 is characterised by wackestone to floatstone with bivalves (of *Pinna* and *Ostrea* type) and brachiopods (Figure 4G,H). Large-sized gastropods, notably *Nerinea*, are observed in lithofacies F6.3. Reworked massive corals as well as platy corals in place are found in lithofacies F6.4 (Figure 3I,J). Shells are sometimes found broken or with separate valves but are most of the time complete. Finally, bioclastic packstones rich in crinoid plates constitute the lithofacies F6.5. These have only been observed in the last two metres of the EST441 well or preserved in bioturbations (Figure 4L).

4.2. Electrofacies Correspondences

A good correspondence between lithofacies and wirelines is observed (Figure 5). Thresholds were applied on GR, PEF and deep resistivity, and allowed to define nine electrofacies (noted EF1 to EF9, Table 2). The correspondence between lithofacies and electrofacies is directly established for massive limestone (F6 = EF2), marly limestone (F5 = EF1), and marlstones with nodules (F4.3 and F4.4 = EF6), for which lithology is the main criterion of differentiation in both methods (Table 2).

In more marly and argillaceous facies, the bulk carbonate content (and, by extension, the EF) is also influenced by the macrofauna (amount and size of bioclasts), while lithofacies are identified based on the type of faunal associations and sedimentary structures. Thereby, a group of correspondences has been established for more marly and argillaceous facies,

for which the amount of calcitic bioclasts has a greater influence on wireline logs than the type of bioclast. In addition, the boundaries between electrofacies are computed thresholds, while the distinction between lithofacies depends on observations; thus, the latter might be less objective, notably in marly lithology. Nevertheless, the classification of marlstones (both in electrofacies and lithofacies) is not crucial for sequence analysis, as their identification is sufficient to delimitate high-frequency sequences. The lithological changes are well expressed in both methods and a similar framework can be established (Table 2).

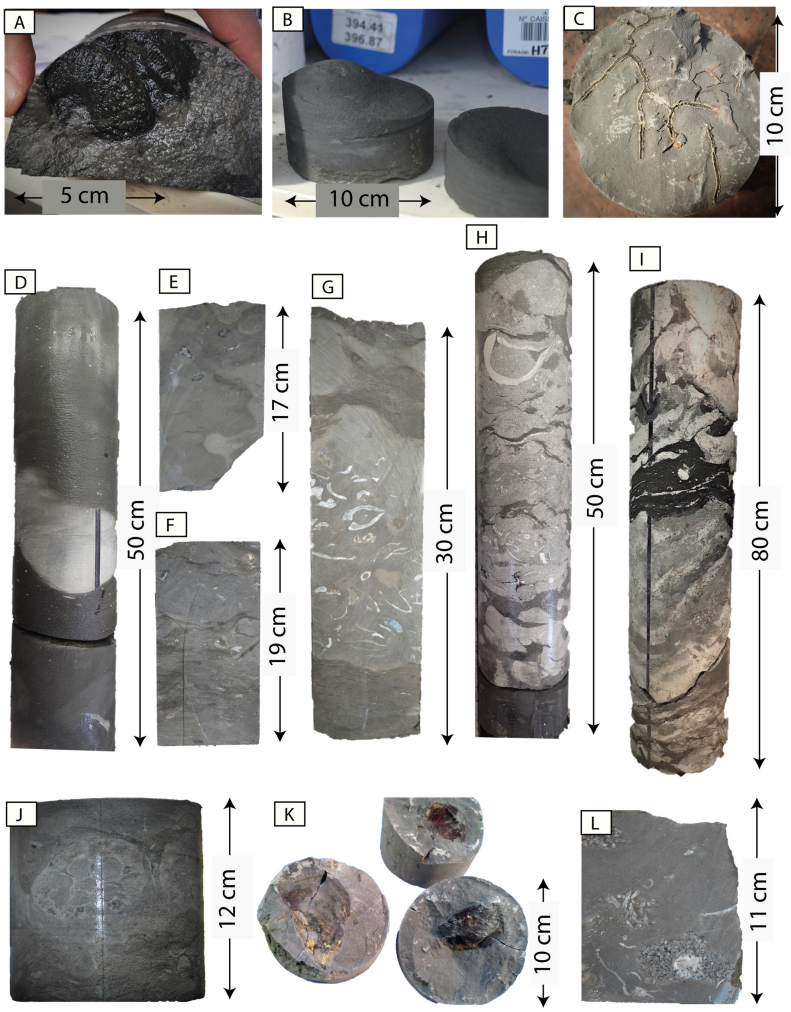

Figure 4. Photographs of notable sedimentological observations and illustrations of facies associations. (**A**) Ammonites observed in lithofacies F2.1, well EST433, −556 m; (**B**) Asymmetrical ripple observed in lithofacies F2.1, well HTM 102, −395.2 m; (**C**) Lithofacies F2.1: silty calcareous claystone with bioturbations of *Chondrites* type, well EST322, −548.65 m; (**D**) Lithofacies F4.4: marlstone with a micritic calcareous nodule showing diagenetic calcite precipitation at its border; well EST423, −403.5 m; (**E**) Bioturbated argillaceous limestone with dissolved oyster shells and silicified serpulids (lithofacies F5.6, BI = 2) (**F**) Bioturbated argillaceous limestone (lithofacies F5.1, BI = 5); (**G**) Lithofacies F6.2 showing a floatstone level containing recrystallised bivalve shells and serpulids, filled with celestine, silica and calcite; well EST433, −562.4 m; (**H**) Lithofacies F6.3: floatstone containing bivalve shells (amongst which *Gryphea*) and numerous gastropods (*Nerinea*), well EST 413, −402.7 m; (**I**) Lithofacies F6.4: platy coral in life position, well EST413, −401.8 m; (**J**) Lithofacies F6.4: floatstone with reworked massive corals, well EST205, −425.75 m; (**K**) Lithofacies F2.2: calcareous claystone showing the superposition of three *Mitilidae* in life position, well EST322, −519.2 m; (**L**); Clayey limestone of lithofacies F5.3 affected by *Thalassinoides* bioturbations, which are infilled by a crinoidal packstone (lithofacies F5.5), well HTM102, −341.8 m.

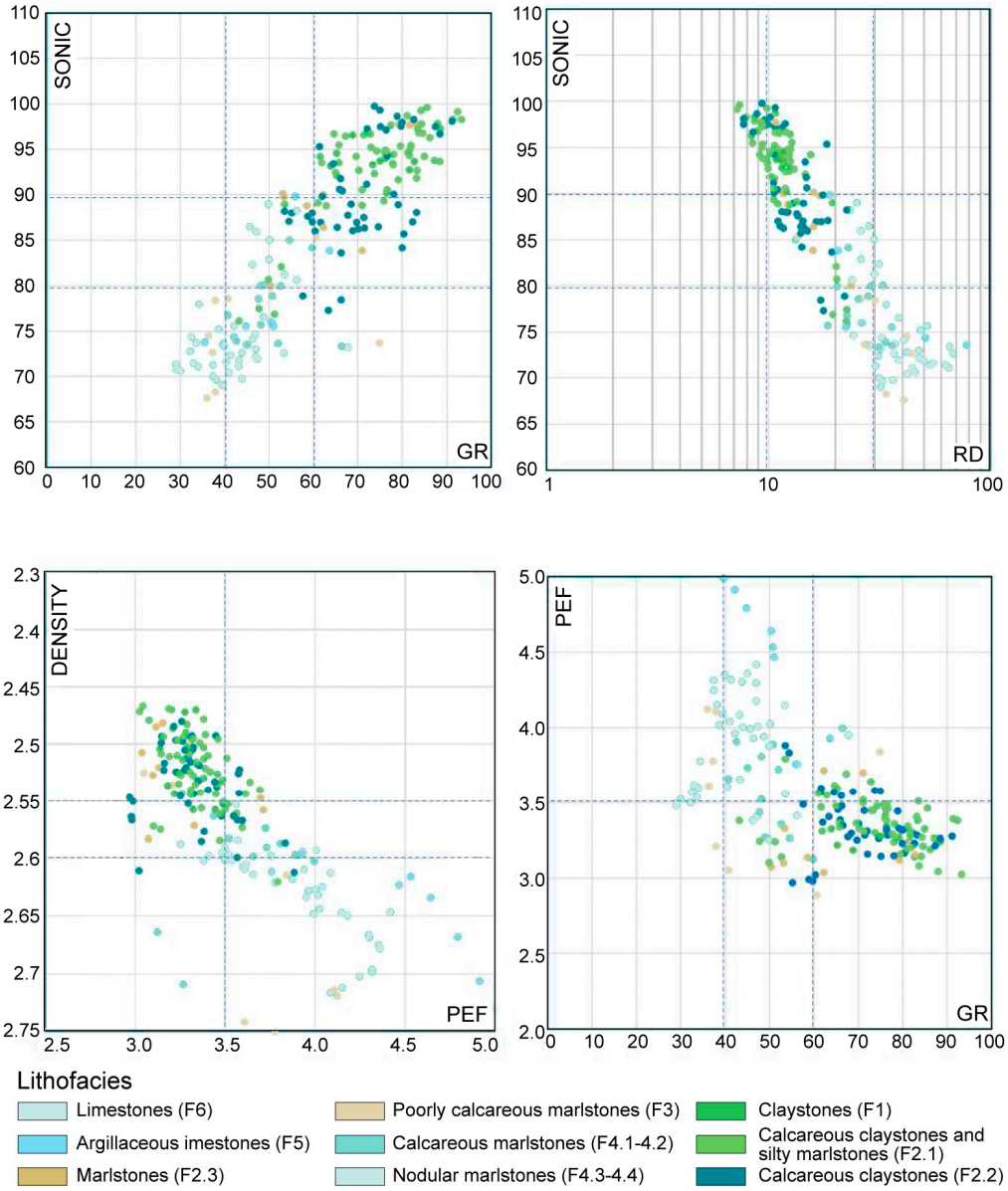

Figure 5. Diagrams in 3D showing the relationship between the wirelines' signals (x and y axes) and lithofacies descriptions (plotted by colour). The DT (Sonic) and density values are well correlated and show redundant information with the GR and PEF values. The most discriminant wirelines for lithofacies determination are GR, DR and PEF.

Table 2. Correspondence between lithofacies and electrofacies.

Applied Thresholds				**EF**	**Lithology**	**Lithofacies**
Limestone	GR < 40	Low resistivity		EF1	Argillaceous limestone	F5
		High resistivity		EF2	Limestone	F6
Marlstone	40 < GR < 60	PEF < 3.5	low resistivity	EF3	Marlstone	F2.3
			high resistivity	EF4	Poorly calcareous marlstone	F3
		PEF > 3.5	RP < 30 ohm.m	EF5	Calcareous marlstone	F4.1–4.2
			RP > 30 ohm.m	EF6	Very calcareous marlstone	F4.3–4.4
Claystone	GR > 60	PEF < 3.5	RP < 10 ohm.m	EF7	Claystone	1
			RP > 10 ohm.m	EF8	Compacted / silty claystone	2.1
		PEF > 3.5		EF9	Calcareous claystone	2.2

5. Interpretations

5.1. Depositional Model

Facies association F1, showing a very argillaceous lithology with discrete horizontal laminations, does not indicate sedimentological evidence for hydrodynamism, which supports that sediment deposition occurred mainly by decantation in a quiet environment below the storm wave base (SWB; Figure 6). The occurrence of frequent *Chondrites* indicates the vicinity of dysoxic environments [75].

Facies association F2, again characterised by bioturbations from the ichnogenus *Chondrites*, indicating low-oxygen environments [75], is marked by a silty fraction and shows some asymmetrical ripples, testifying to currents of low energy (lithofacies F2.1; Figure 4B). Given the proximity of dysoxic areas, these facies are attributed to geostrophic currents or storm deposits [76,77]. Therefore, the abundance of *Chondrites* and the scarcity of bioclasts in lithofacies F2.1 indicate that F2.1 is relatively distal compared to other lithofacies. A slight increase in lime mud is noticed in lithofacies F2.3. These marly deposits are strongly bioturbated and frequently show the ichnogenus *Rhizocorallium*. After [78], the short size and subvertical shape of most specimens might indicate the fossil trace of a suspension-feeding organism on a firmground substrate. Lithofacies F2.3. is thus interpreted as a slightly shallower environment in outer ramp settings (Figure 6).

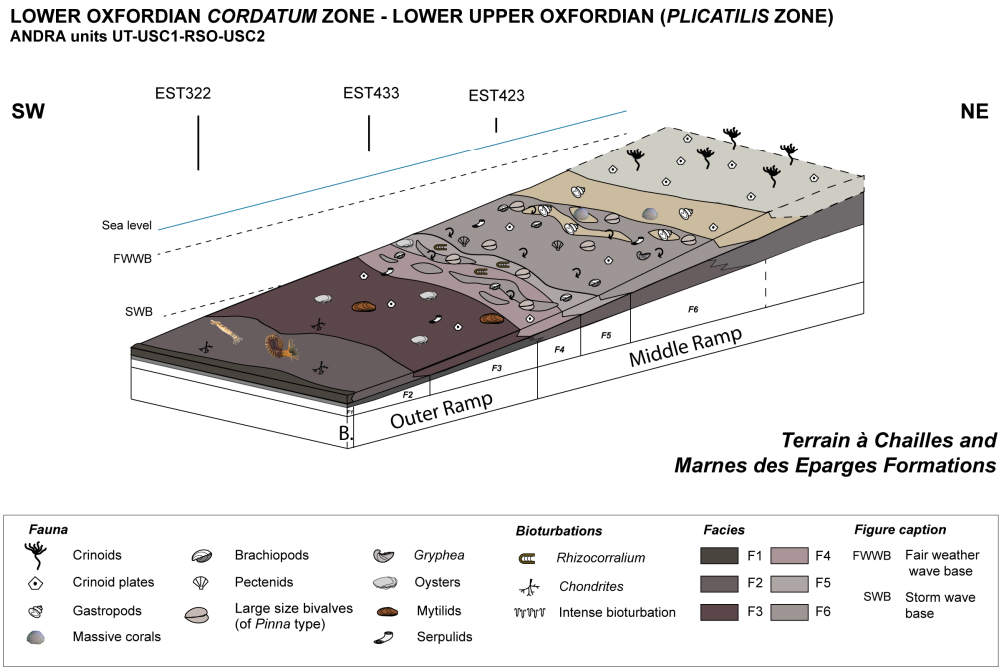

Figure 6. Depositional model of lower and upper Oxfordian deposits (*cordatum* to *plicatilis* zones). Depositional environments show a progressive deepening towards the SO, typifying a homoclinal ramp morphology. Numbers F1–F6 indicate the five facies association recognised; B. stands for Basin.

Facies association F3 shows HCS, which is attributed to storm waves and current influences. The ramp model of [79–81] outlines the outer ramp from the middle ramp based on the frequency of storm deposits. Therefore, F3 is rather attributed to an outer ramp depositional environment. Facies association F4 is characterised by frequent reworking, typifying a middle ramp depositional environment. The good preservation state of bivalve shells, corals and gastropod shells of F4 indicates, however, a limited winnowing (Figure 6).

The transition to more proximal environments continues either with a rather in-situ sedimentation documented by the marly limestones (F5), or by the occurrence of reworked calcareous deposits containing abundant macrofauna, including brachiopods, bivalves, gastropods and corals (F6). A zonation of the benthic macrofauna can be identified across the ramp. Oysters, often colonised by serpulids, constitute the first calcareous benthic

macrofauna observed in the distal part of the ramp (F3). They are followed by the settlement of abundant brachiopods (amongst which are rynchonellids) and bivalves (such as *Pinna* and pectenids). These organisms are rather suspension-feeders, indicating nutrient-rich waters. In the most proximal part, thick-walled bivalves (*Gryphea*), gastropods and massive corals are found. The occurrence of massive and platy corals suggests lower nutrient rates and seawater environments close to the photic zone.

All investigated wells show that a lithological transition occurs within the "Terrain à Chailles" Formation. In the lower part of the formation, lithofacies show little variation. These are mostly linked to changes in quartz (silt fraction) and carbonate contents and correspond to outer ramp settings. In contrast, the upper part of the "Terrain à Chailles" Formation and the "Marnes des Eparges" Formation show an increased occurrence of calcareous beds and benthic organisms with a higher diversity in benthic macrofauna. Paleoenvironments thus evolve towards middle ramp settings.

5.2. High-Frequency Sequences

In the lower part of the "Terrain à Chailles" Formation, mfs are placed in the most argillaceous deposits (F1/EF7) and fs are at the top of the most calcareous deposits (F2.3/EF8-EF9) based on DT and GR trends (Figure 7). The latter deposits are characterised by intense bioturbation accompanied, in some cases, by the occurrence of short-shaped *Rhizocorallium*. This may indicate the incomplete development of firmgrounds [78] and highlights reduced sedimentation rates at fs.

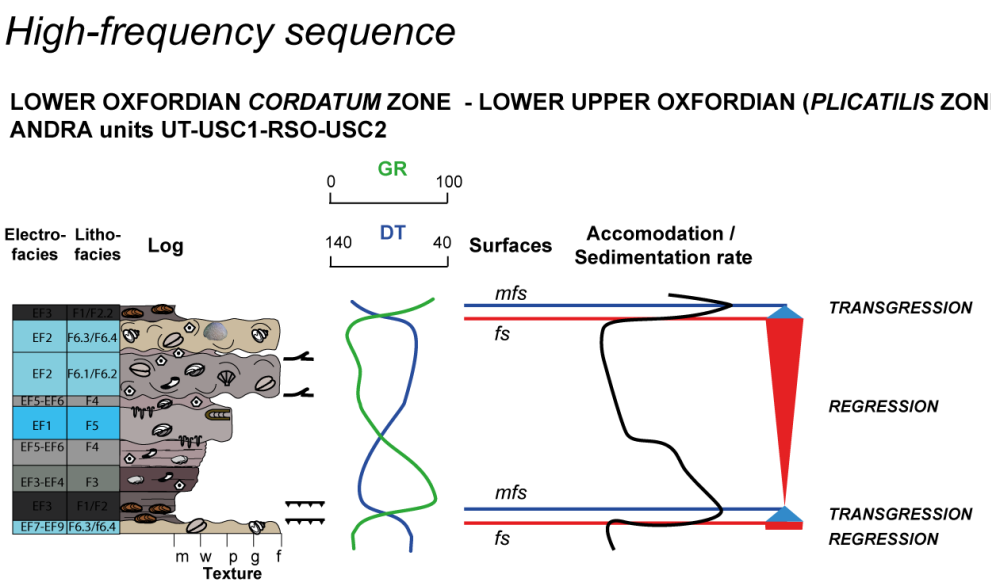

Figure 7. Scheme of typical high-frequency sequences (lithofacies, electrofacies, GR, DT) in the uppermost Lower Oxfordian/lowermost Middle Oxfordian deposits.

In the upper part of the "Terrain à Chailles" Formation and in the "Marnes des Eparges" Formation, mfs are also placed in the most argillaceous deposits (F1/EF7-EF9), and fs in the most calcareous deposits (F6/EF2) based on DT and GR trends (Figure 7). The stack of epibenthic Mytilidae bivalves in life position likely illustrates reduced sedimentation rates and the occurrence of firmgrounds. Firmground occurrences tend to show a certain pattern: they are absent in the lower part of the "Terrain à Chailles" Formation, found in mfs in the upper part of the "Terrain à Chailles" Formation, and they are mixed with fs in the two high-frequency sequences that precede major surfaces RL1 and RL2.

The Mfs are marked by positive GR and DT peaks. A progressive joint decrease in GR and DT characterise shallowing-upward trends until they reach minimum values corresponding to fs. The amplitude of GR and DT variations is smaller in the lower part of

the "Terrain à Chailles" Formation (50 API and 50 ms.ft^{-1}) compared to the upper part of the "Terrain à Chailles" Formation (100 API and 100 ms.ft^{-1} respectively).

High-frequency cycles are characterised by facies associations evolving from F1 to F6. They are typically marked by a short decrease, followed by a progressive increase in carbonate content, well recorded in the GR and DT wirelines (Figure 7). High-frequency cycles are therefore less expressed in the lower part of the "Terrain à Chailles" Formation, where facies associations F5 and F6 are not present.

5.3. Correlation of Wells

Noticeable sedimentary features and DT/GR changes allowed remarkable levels to be defined, which were used for correlation between wells. Amongst remarkable levels (RL), a maximum carbonate content can be correlated in the nine wells at the boundary between the "Terrain à Chailles" and "Marnes des Eparges" formations. This remarkable level is indicated as RL1 (Figure 8).

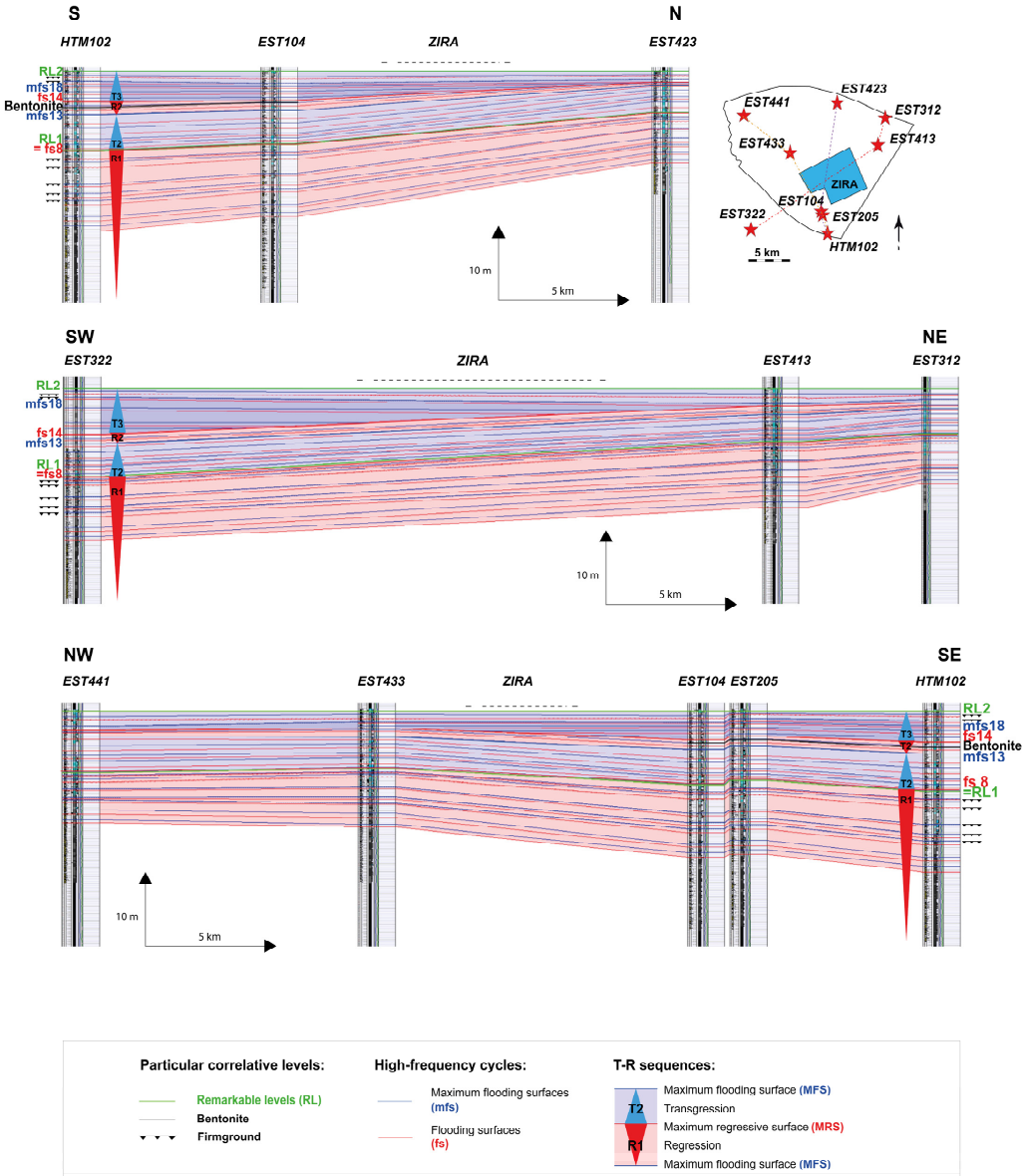

Figure 8. Correlation of the nine wells investigated around the ZIRA based on the main remarkable surfaces. Wells have been horizontalised on surface RS2.

A second remarkable level (RL2) is identified at the top of the "Marnes des Eparges" Formation. It consists of a level of floatstone (F6) showing bioturbations filled by crinoid ossicles (Figure 4L) observed in wells HTM102, EST433, EST205 and EST104. In well EST413, these bioturbations occur in floatstone and framestone levels with platy corals, indicating the beginning of the overlying "Marnes et Calcaires à Coraux de Foug" Formation. In well EST423, similar boundstone facies is noticed but bioturbations with crinoids were not observed. RL2 is more calcareous than the underlying deposits. In addition, levels of firmground showing accumulation of epibenthic bivalves in life positions were observed on cores at different stratigraphic levels and used for correlation.

Twenty cycles of high frequency have been identified and correlated (Figure 8). The boundary between the *mariae* and *cordatum* ammonite zones (Lower Oxfordian), identified between the surfaces mfs8 and mfs9 in well EST322, was then extended in the other wells. Similarly, the boundary between the *cordatum* and the *plicatilis* zones, defining the Lower-Middle Oxfordian boundary, occurs between fs8 and fs9 in wells EST322 and HTM102. The stacking pattern of the high-frequency sequences allowed for defining three transgressive-regressive cycles of lower frequency (higher rank).

5.4. Transgressive Regressive Sequence and Architecture of Sedimentary Deposits

The correlation of wells allows for delineating three transgressive-regressive sequences. The first MRS of the third order (corresponding to fs8) marks the end of a long-term regressive pattern. It is marked by a maximum carbonate content well expressed in the GR and DT records and corresponds to the maximum progradation of proximal deposits (facies association F6) in the most distal part of the study area (well EST322).

The second MRS of the third order corresponds to fs14 and marks a change in deposit geometries. Above this surface, three high-frequency cycles are recorded only in most distal parts of the ZIRA (i.e., numbered 15, 16 and 17 in wells EST104, EST205, HTM102, EST322). The thickness of these three cycles is higher in the distal wells (i.e., of 4.7 and 2.6 m in EST322 and HTM102, respectively), and slightly decreases in wells EST104 and EST 205 (towards 2.2 and 2.0 m, respectively), until these units disappear in the proximal areas (i.e., wells EST 433, EST 441, EST423, EST413 and EST 312), forming an onlapping body.

MRS1 and MRS2 terminate regressive deposits R1 and R2 and likely represent the maxima of regression of sequences of lower rank. The MFS of the second sequence is placed in the most argillaceous deposits, recorded by higher GR values (Figure 8). It corresponds to mfs13 and pinpoints the end of the second transgressive phase (T2). This is in accordance with previous studies on borehole HTM102 [20,21] (cf. Figure 3).

The MFS of the third sequence could either be placed: (1) at a second maximum in clay content in the interval (mfs18) or (2) in the return of homogeneous calcareous deposits at the regional scale, possibly located higher up in the succession [13,14,82,83]. The study of deposits higher up in succession (Middle Oxfordian) is thereby needed to further constrain T3.

6. Discussion

6.1. Accommodation Changes Driven by Sea Level Variations

The stratigraphic sequences highlighted in this work can be compared to other stratigraphic frameworks established at larger scales in the eastern part of the Paris Basin [13,14,59], the entire basin and elsewhere [6,44,84].

- *Regressive deposits (R1)*

In the eastern part of the Paris Basin, the "Terrain à Chailles" Formation, which is assigned to the Lower Oxfordian *mariae* and *cordatum* ammonite zones and corresponds to the R1, has a duration of 0.8 Myr, according to correlations with the geological time scale [84,85]. The MRS is marked by the surface RL1 (equivalent to fs8, Figures 8 and 9), which corresponds to a regional sequence boundary (named LJII by [13], S2 by [16] and S3 by [14]). This surface corresponds to the 161 Myr "medium or minor cycle boundary" termed JOx2 of [84] and may represent the sequence boundary of 3rd order Ox2 of [44]. The

regressive trend of the "Terrain à Chailles" Formation is therefore interpreted as recording an eustatic sea-level decrease.

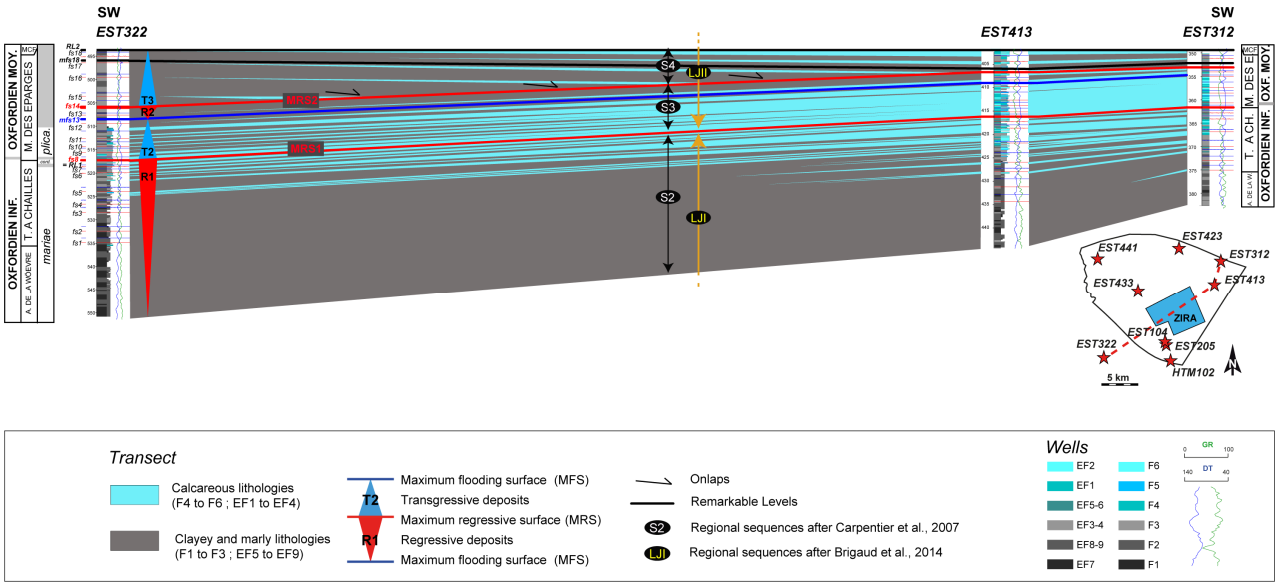

Figure 9. Correlations on an NE-SW transect (wells EST322–EST413–EST312) showing lithological evolution and transgression/regression cycles. Litho and electrofacies have been grouped into calcareous deposits (from nodular marlstone to massive limestone in blue) and clayey deposits (clays, silty calcareous clays and bioclastic marlstone in grey). Wells have been horizontalised on surface RL2.

The low thickness attributed to the *cordatum* ammonite zone (two to three metres in the various parts of the ZIRA), although ammonite biostratigraphy for this interval is not well documented, suggests the occurrence of a major hiatus and a possible sequence boundary gathered with RL1. However, clear evidence supporting the occurrence of a sea level fall discontinuity (e.g., major change in geometry, a major erosive surface, abrupt facies change towards proximal deposits in distal settings or exposure features) in proximal settings is lacking in this mid-outer ramp domain. Nevertheless, such a stack of surfaces implies that an LNR is missing in the study area. Studies carried on a wider scale in the eastern Paris Basin have not evidenced any LNR in the more distal part of the Basin [13,14].

Therefore, it is possible that the top of R1 records an HNR, followed by a highly condensed LNR [3,71]. This hypothesis is supported by the work of [14] and [86]. In Switzerland, a sharp contact at the base of a 1.5- to 2.5-metre-thick carbonate bedset that contains abundant bivalves, notably *Pholadomya protei*, is interpreted as a sea-level fall. Our observations show that *Pholadomya* are present at fs10 in well EST441, at fs9 in well EST423, at fs12, 13 and 18 in well EST413 and at fs3 in well EST104. Therefore, in the ZIRA, although *Pholadomya* are observed in some wackestone to floatstone deposits of facies association F6, they rather indicate an induration of substrate during transgressive surfaces than sea level fall discontinuities, additionally pointing to generally low sedimentation rates.

The preservation of an LNR at the top of R1 might be indicated by 3 metres thickening of the interval corresponding to the high-frequency cycles 5 to 7 in the SE direction (towards the basin, Figure 9). A correlative conformity might be placed where dismantling facies first appear (lithofacies F6.2 to F6.4). These beds are found in the cycle of high-frequency 4 and are well expressed in most proximal wells (EST413, EST423 and EST441). They evolve basinward towards nodular marlstones with bivalves and brachiopods in wells EST104 and EST205 (lithofacies F4.3 and 4.4) and towards clayey-silty limestone with crinoid plates (classified in lithofacies F5.2) in EST322. However, basinward thickening seems to start slightly above this surface (Figure 8).

Another possibility is that the LNR of this sequence is dominated by siliciclastic deposits, as is classically assumed for mixed carbonate-siliciclastic ramps [67,83] and as is observed in equivalent deposits from Spain [87]. However, such quartz-rich facies are not observed in wells located in the more distal part of the ZT.

LNR deposits are not always well expressed in ramp settings, as their thickness and texture are highly dependent on the amplitude of the relative sea level fall [67]. The small thickness of the *cordatum* ammonite zone may either indicate a major hiatus or a highly condensed interval. In the absence of sedimentary features characteristics of emersion or net shallowing up (karstic features, paleosols, or shoreface or lagoonal environments), condensation is preferred here. It could occur either during a potential LNR (as a result of low sedimentation rates between dismantling facies) or during the following relative sea level rise (T2, Figure 9). In the latter case, however, a strong shift of depocentres towards the proximal part of the basins would be expected and is not, for instance, observed.

- *Transgressive deposits T2 and regressive deposits R2*

This interval has a relative constant thickness over the ZIRA (between 8 and 12 metres) and corresponds to the S3 sequence of [14] (Figures 8 and 9). The MFS at the end of T2 is marked by a maximum in the clay content (observed in lithofacies and the GR record), corresponding to mfs13. At the regional scale, if the correlations are correct, the thickness of this sequence is highly variable. Sequence S3 is well developed 50 km westward and north-westward of the ZIRA (with thicknesses reaching 80 m), while it is absent 15 km north of the ZIRA. Ref. [14] attribute these regional differences to the accommodation/sedimentation ratio variation. As a tectonic interplay has not been evidenced in this study, the transgressive–regressive interval T2–R2 is attributed to sea-level changes.

6.2. Local Tectonics and Inherited Paleotopography

The regressive interval R2 ends in the ZIRA with a second maximum regressive surface (placed at fs14, equivalent to the S2b surface of [16], which corresponds to a change in the geometry of deposits, as onlaps are identified above the MRS. This change in deposit geometries is not associated with major facies changes at the ZIRA scale. This surface may be correlated to the sequence boundary of sequence S4 of [14] (Figure 9), which marks the boundary between the *vertebrale* and the *antecedens* ammonite subzones in the Middle Oxfordian *plicatilis* ammonite zone. Our transects indicate the occurrence of differential subsidence within sequence S4 (Figure 9), with enhanced subsidence towards the basin (SW) compared to other sequences. This feature could be linked to extensive tectonics according to the activity of the Metz Hercynian fault, which likely created a hill in the Senonville area (about 50 km in the NE, Figures 1 and 2), and a locally intermittent subsidence towards the SW [6,30,32–34].

In the regressive interval R1 (Lower Oxfordian), bedsets settle on an inherited topography created by the underlying clayey sediments of the Cox [40,88]. Our data support the occurrence of a relatively constant slope showing a slightly convex shape with slightly steeper relief in the NE part of the basin (Figure 9). The slightly convex shape is likely attributed to the distal downlaps of underlying muscles of progradation of the Cox and might point to a gentle slope break typical of ramps on prograding clastics (belonging to the distally steepened ramp, following [89].

The slope angle is a determining factor that controls the facies and geometries of overlying deposits. In this case study, high-energy deposits laterally equivalent to the mud-rich deposits of the "Terrain à Chailles" and "Marnes des Eparges" formations are only located seventy kilometres northward of the ZT and are constituted by the oolitic facies of the "Oolithe de Senonville" Formation [14]. The restriction of coarse deposits to the euphotic and hydrodynamic zones, and the spread of muddy and silty deposits in euphotic settings, is very typical of a "low energy ramp" with a gentle slope [67,89,90].

In addition, the occurrence of a gently dipping slope equally has an influence on the morphologies of sedimentary deposits. During relative sea level drops, it limits the extent of subaerial exposure areas and restricts the power of reworking processes [67,91].

Consequently (and contrary to rimmed platform morphologies), the record of LNR deposits strongly depends on the amplitude of the relative sea level change. Alternatively, relative sea level rises typically gently affect dipping ramps by generating condensation [67], which explains the occurrence of an important hiatus at RL1 (where most of the *cordatum* ammonite zone is missing).

A (slightly distally steepened) ramp on prograding clastics morphology (sensu [89]) is observed in the whole studied succession up to the remarkable level RL2. This level marks the settlement of the coral reefs of the "Marnes à Coraux de Foug" Formation, which might sign a switch towards a shallow ramp and downslope buildups, and later evolve towards a rimmed shelf morphology during the Middle Oxfordian [13,14,89].

6.3. Paleoenvironmental Changes through the Lower–Middle Oxfordian Boundary

The change from a muddy siliciclastic sedimentation towards a carbonate platform system is well known through the Early–Middle Oxfordian boundary in the North Tethyan domain (Brigaud, Ferry). Regional stratigraphic works carried out in the western and eastern Paris Basin highlight the settlement of a reefal barrier in the Middle Oxfordian [9,13,14,16]. In an indirect manner, palaeontological studies report equally the extension of coral reefs in the Middle Oxfordian [92,93], marking the extension of rimmed carbonate shelves at low latitudes after their demise during the Late Callovian and Early Oxfordian. However, very few studies have detailed the transitional stages between the clay lobe system and the carbonate-rimmed shelf at that time interval [14].

In this study, a stepwise return of carbonate production after the Late Callovian and Early Oxfordian carbonate crises is documented. The initiation of the recovery is witnessed by the deposition of the first sedimentary bodies containing a diversified carbonate-producing fauna (brachiopods, bivalves and a few crinoids). These are found in the upper part of the regressive interval R1 (of Early Oxfordian age, *mariae* ammonite zone, *praecordatum* subzone). Calcified organisms are dominated by suspension–feeding fauna, typical of a heterozoan factory, and indicating high rates of nutrients in ocean waters [94–96].

The bedsets at the base of the "Marnes des Eparges" Formation, deposited during the *plicatilis* Zone (Middle Oxfordian), show the settlement of the first massive corals and contain abundant crinoid plates, reaching a further step in the colonisation and diversification of carbonate-producing organisms. Although massive corals are organisms living symbiotically with photosynthetic organisms and living in oligotrophic waters, they are less sensitive to turbidity than other hermatypic corals [97,98]. Their association with suspension-feeding organisms, such as crinoids, may indicate a slight decrease in water turbidity.

A further step in the recovery of carbonates occurred later in the Middle Oxfordian. The settlement of platy corals in the "Marnes à Coraux de Foug" Formation and higher up in the "Calcaires à Coraux de Foug" Formation initiates a change in the margin topography towards a rimmed shelf by adopting a shallow ramp and downslope buildup morphology [13,89]. The switch towards a photozoan carbonate production mode occurring during the Middle Oxfordian documents here the climax of a long-term decrease in detrital fluxes towards seawaters.

Sedimentary deposits evolve from a homoclinal ramp towards a distally steepened ramp at the regional scale (NE Paris Basin [14]). Similar changes have been documented in Switzerland [86,99], where deposits very similar to the NE Paris Basin are found (e.g., marl-limestone alternation with brachiopods and bivalves, [99], in certain sections in Spain poorly affected by tectonics [87] and in Uzbekistan [50]. Despite various tectonic contexts, the extensive growth of carbonate reefs during the Middle Oxfordian is equally documented in the Atlantic Ocean (Alabama, [100]), pinpointing the extent of the recovery of the carbonate factory at tropical paleolatitudes.

6.4. Impact of Climate Variations on the Sedimentary Record

- *Long-term climate evolution*

Previous studies performed in the eastern Paris Basin have shown that drier climatic conditions take place during the Early Oxfordian [20,48,101], likely leading to reduced weathering and lowering continental fluxes towards the ocean. The decrease in humidity, however, is either documented from the "Argiles de la Woevre" Formation (corresponding to earlymost Oxfordian *mariae* Zone, *scarburgense* subzone) or from the "Terrain à Chailles" Formation where the first calcareous beds are observed (i.e., later in the Early Oxfordian, in the *mariae-cordatum* ammonite zone boundary) depending on the used proxy (clay mineralogy or terrestrial biomarkers). From clay mineralogical data, more humid conditions deduced from the reappearance of kaolinite are likely recorded in the *transversarium* zone in the Eastern Paris Basin above the "Marnes des Eparges" Formation (i.e., "Marnes et Calcaires à coraux de Foug" Formation). In the studied interval, clay mineral evolution is relatively homogeneous and mainly composed of smectite and illite, suggesting a semi-arid climate with contrasting seasons (Figure 3).

Moreover, a 3 °C increase in seawater temperatures is recorded by the $\delta^{18}O$ values of oysters and brachiopods through the Lower-Middle Oxfordian boundary (*cordatum–transversarium* ammonite zones [47]. Therefore, the stratigraphic scheme built in this study shows that the initiation of carbonate recovery (in the uppermost *mariae* ammonite zone, *praecordatum* subzone) occurs during the onset of a climatic shift from cool and arid conditions (i.e., Lower Oxfordian) to more humid and warm conditions (i.e., Middle Oxfordian).

In addition, the recovery of carbonate production is associated with transgressive and highstand normal regressive deposits [2,3]. The stepwise relative sea-level rise likely triggered the gradual flooding of Tethyan margins and the progressive diversification of carbonate producers in the context of low weathering and continental runoff [48,101]. This hypothesis is coherent with mixed silicilastics–carbonate ramp models [2,67,83] and stratigraphic works on deposits from the Lower-Middle Oxfordian transition in the western Tethys [87].

- *Climate cyclicities of high frequency*

Eight sequences of high frequency have been interpreted in the "Terrain à Chailles" Formation, which has a duration of 0.8 Myr, by correlation with [85]. Therefore, each high-frequency sequence represents a duration of 0.1 Myr, which is consistent with a rhythmicity of fourth to fifth order, and a sedimentation controlled by Milankovitch cyclicities [102,103]. An orbital trigger tuned by precession and eccentricity cycles has already been inferred for shallow water Oxfordian deposits from sedimentological analyses in the Jura domain mountains [102,104]. In addition, the record of the 100-kyr, 405-kyr, and possibly the 2.4-myr eccentricity cycles is obtained from the $\delta^{13}C$ and $\delta^{18}O$ signals of the bulk carbonate during the Lower Oxfordian in the same Andra Borehole [45] and confirms that Milankovitch cycles likely influenced sedimentation around the Lower/Middle Oxfordian transition. The good correspondence between the stratigraphic scheme proposed in this study and the GTS [85] is, however, explained by the lithological similarity and the (palaeo)geographical proximity between our site of study and the site of reference used in the GTS (outer ramp deposits of Switzerland, after [86]. Therefore, it is possible that the duration of the *cordatum* and *plicatilis* zones is underestimated in the GTS, as a condensed surface has been identified at the top of the "Terrain à Chailles" Formation (MRS1).

High-frequency sequences reflect relative sea-level variations. Changes in orbital parameters trigger changes in insolation, which generate sea-level variations via various mechanisms. During cool time intervals, these variations are principally triggered by the wanning and waxing of polar ice [105], while during warmer time intervals, they are interpreted to reflect changes in water temperature and volume of ocean waters and water retention and release in lakes and aquifers [106–108]. Although the occurrence of limited polar ice caps is discussed for the Oxfordian [107–109], their volume was likely too small to induce glacio-eustatic variations [102,110].

In addition, high-frequency cycles are characterised by enhanced detrital content during relative sea level rises and carbonate-dominated sedimentation during relative sea-level falls. This does not support the occurrence of changes in water volume linked to

insolation changes, as colder time intervals would rather be associated with relative sea level falls.

Milankovitch-paced marl-limestone alternations are also interpreted as directly reflecting short-term climate fluctuations by inducing high-frequency changes in humidity and nutrient input in the ocean [111]. However, a higher detrital input would be expected during warmer time intervals, which is not in adequation with the general environmental transition that occurs through the Lower Middle Oxfordian boundary, where a siliciclastic-dominated shelf with cool and arid conditions evolves towards a carbonate shelf with a warmer and more humid climate.

An alternative hypothesis is that orbitally driven changes in insolation triggered changes in temperature and climate that modulated relative sea level via the storage of water in aquifers during more humid phases. Aquifer-eustasy is indeed increasingly viewed as a controlling factor for third to fifth order sequences during time periods devoid of polar ice, given its amplitude and the retention time of water in aquifers (10^4 to 10^5 years; [108,112–115]. During warmer and more humid phases, water is stored, and the relative sea level decreases. Conversely, during colder and more arid phases, the relative sea level rises due to the discharge of aquifers. In parallel, orbitally driven changes in temperature likely modulate carbonate production with warmer phases, leading to enhanced carbonate production [111]. Such climatic alternations suggest a highly contrasted seasonal climate governed by humidity–aridity phase oscillations. This is in agreement with the nature of clay minerals found in the basin (e.g., smectites), which formed in nearby continental landmasses at that time and with maximal eccentricity periods recognised during the Late Jurassic [116].

7. Conclusions

The vertical and lateral evolutions of sedimentary facies of the "Terrain à Chailles" and "Marnes des Eparges" formations were investigated across the ZIRA. Nine wells were correlated based on their lithofacies and petrological properties (GR, DT and electrofacies based on a combination of GR, PEF and deep resistivity), allowing a resolution better than a metre. The new sequence stratigraphic framework established in this work has been combined with previous biostratigraphic work to provide robust (supra)regional correlations. A basinward shift of depocenters has been identified in the "Marnes des Eparges" Formation (Middle Oxfordian age). This has no influence on rock properties, as this is not associated with any facies change. The gently deeping slope in the SW direction occurring at the base of the "Terrain à Chailles" Formation indicates a slightly distally steepened ramp prograding on siliciclastics. This impacted depositional geometries, as a general "stack of plates" pattern is documented at the ZIRA scale. The interplay between sea-level variations and climatic oscillations during sediment deposition are other factors that influence lithological properties in the subsurface by controlling the relative amount of terrigenous fluxes and carbonate production. A stepwise increase in carbonate production is observed in the "Terrain à Chailles" Formation (Early Oxfordian age), starting in the uppermost *mariae* ammonite zone, which is marked by an increase in the frequency of marl limestone alternations and the appearance of the first calcareous fauna of brachiopods and bivalves. A second step is reached at the base of the "Marnes des Eparges" Formation (close to the Lower-Middle Oxfordian boundary, *cordatum–plicatilis* ammonite zones boundary), where a few massive corals are found. A further step is documented with the settlement of coral buildups in the "Marnes à Coraux de Foug" Formation (later in the Middle Oxfordian).

EF was useful for completing the stratigraphic model in uncored intervals. More generally, this study shows that wireline-based and sedimentological logs allow us to bring complementary insights to constrain a stratigraphical model. EF are based on an objective classification and are more affected by the amount of bioclasts than by their nature. Correlations based on EF (and wirelines in general) depend on the resolution of the tools: usually 0.5 m and 1.0 m for GR and DT, respectively. The sedimentological part of this study allowed us to obtain a sedimentological log at a better resolution (centimetric), qualitative

information on the faunal content and the building of a depositional model. The counterpart is a less quantitative view of lithological heterogeneities. Therefore, the reconstruction of paleoenvironments not only allows predicting lithologies by the building of depositional models but also permits precising wire well log signals. Reciprocally, electrofacies (based on GR, PEF and deep resistivity wireline logs) have given an estimation of the proportion and size of calcareous bioclasts, which is linked to the recovery of carbonate production and paleoenvironmental changes, and which can equally be used to predict geomechanical properties in the subsurface.

This new stratigraphical model additionally details the modality of the carbonate recovery after the Late Callovian—Early Oxfordian carbonate crisis, providing insights on the role of local and supra-regional parameters, such as eustatism, topography, tectonics and climate, on the evolution of the geometry, heterogeneity and faunal content of sedimentary bodies in a transitional interval between muddy-siliciclastic and reefal carbonate series.

Author Contributions: Conceptualisation, P.L. and F.S.; methodology, F.S.; validation, B.V. and P.P.; formal analysis, B.V., P.P. and C.M.; investigation, C.M, F.S. and F.D.; resources, F.S. and P.L.; writing—original draft preparation, C.M..; writing—review and editing, C.M., P.P. and B.V.; visualisation, C.M.; supervision, F.S. and P.L.; project administration, F.S.; funding acquisition, F.S. All authors have read and agreed to the published version of the manuscript.

Funding: This research was supported by the "Agence Nationale pour la Gestion des Déchets Radioactifs" (Andra–French National Radioactive Waste Management) and funded by INGEN: Innovations for Geosciences.

Data Availability Statement: Not applicable. Data available in a publicly accessible repository that does not issue DOIs. Publicly available datasets were analysed in this study. This data can be found here: https://international.andra.fr/documents-and-visual-ressources.

Acknowledgments: The authors are grateful to the French Nuclear Agency for Nuclear Waste Storage (ANDRA) for the founding of the project and the authorization to freely communicate our results. We would like to particularly thank Claude Aurière for the access to cores and wells data. Three anonymous reviewers are acknowledged for their constructive comments.

Conflicts of Interest: The authors declare no conflict of interest. The funders had no role in the collection, analyses, or interpretation of data; in the writing of the manuscript; or in the decision to publish the results.

References

1. Catuneanu, O. Model-independent sequence stratigraphy. *Earth-Sci. Rev.* **2018**, *188*, 312–388. [CrossRef]
2. Catuneanu, O. Sequence Stratigraphy: Guidelines for a Standard Methodology. *Stratigr. Timescales* **2017**, *2*, 1–57. [CrossRef]
3. Catuneanu, O.; Abreu, V.; Bhattacharya, J.; Blum, M.; Dalrymple, R.; Eriksson, P.; Fielding, C.; Fisher, W.; Galloway, W.; Gibling, M.; et al. Towards the standardization of sequence stratigraphy. *Earth-Sci. Rev.* **2009**, *92*, 1–33. [CrossRef]
4. Bourquin, S.; Guillocheau, F. Keuper stratigraphic cycles in the Paris basin and comparison with cycles in other peritethyan basins (German basin and Bresse-Jura basin). *Sediment. Geol.* **1996**, *105*, 159–182. [CrossRef]
5. Bourquin, S.; Robin, C.; Guillocheau, F.; Gaulier, J.-M. Three-dimensional accommodation analysis of the Keuper of the Paris Basin: Discrimination between tectonics, eustasy and sediment supply in the stratigraphic record. *Mar. Pet. Geol.* **2002**, *19*, 469–498. [CrossRef]
6. Guillocheau, F. Mise en évidence de grands cycles transgression-régression d'origine tectonique dans les sédiments mésozoïques du Bassin de Paris. Comptes rendus de l'Académie des sciences. *Série 2 Mécanique Phys. Chim. Sci. L'univers Sci. Terre* **1991**, *312*, 1587–1593.
7. Brigaud, B.; Durlet, C.; Deconinck, J.-F.; Vincent, B.; Pucéat, E.; Thierry, J.; Trouiller, A. Facies and climate/environmental changes recorded on a carbonate ramp: A sedimentological and geochemical approach on Middle Jurassic carbonates (Paris Basin, France). *Sediment. Geol.* **2009**, *222*, 181–206. [CrossRef]
8. Brigaud, B.; Vincent, B.; Durlet, C.; Deconinck, J.-F.; Blanc, P.; Trouiller, A. Acoustic Properties of Ancient Shallow-Marine Carbonates: Effects of Depositional Environments and Diagenetic Processes (Middle Jurassic, Paris Basin, France). *J. Sediment. Res.* **2010**, *80*, 791–807. [CrossRef]
9. Andrieu, S.; Brigaud, B.; Barbarand, J.; Lasseur, E.; Saucède, T. Disentangling the control of tectonics, eustasy, trophic conditions and climate on shallow-marine carbonate production during the Aalenian–Oxfordian interval: From the western France platform to the western Tethyan domain. *Sediment. Geol.* **2016**, *345*, 54–84. [CrossRef]

10. Lasseur, E. La Craie du Bassin de Paris (Cénomanien-Campanien, Crétacé Supérieur). Sédimentologie de Faciès, Stratigraphie Séquentielle et Géométrie 3D. Ph.D. Thesis, Université de Rennes 1, Rennes, France, 2007.
11. Robaszynski, F.; Pomerol, B.; Masure, E.; Bellier, J.-P.; Deconinck, J.-F. Stratigraphy and stage boundaries in reference sections of the Upper Cretaceous Chalk in the east of the Paris Basin: The "Craie 700" Provins boreholes. *Cretac. Res.* **2005**, *26*, 157–169. [CrossRef]
12. Guillocheau, F.; Robin, C.; Grosdoy, B.; Hanot, F.; Lestrat, P.; Mettraux, M. Évolution géodynamique du Bassin de Paris: Apport d'une base de données stratigraphiques 3D. *Bull. D'information Géologues Bassin Paris* **1999**, *36*, 3–35.
13. Brigaud, B.; Vincent, B.; Carpentier, C.; Robin, C.; Guillocheau, F.; Yven, B.; Huret, E. Growth and demise of the Jurassic carbonate platform in the intracratonic Paris Basin (France): Interplay of climate change, eustasy and tectonics. *Mar. Pet. Geol.* **2014**, *53*, 3–29. [CrossRef]
14. Carpentier, C.; Lathuilière, B.; Ferry, S.; Sausse, J. Sequence stratigraphy and tectonosedimentary history of the Upper Jurassic of the Eastern Paris Basin (Lower and Middle Oxfordian, Northeastern France). *Sediment. Geol.* **2007**, *197*, 235–266. [CrossRef]
15. Carpentier, C.; Martin-Garin, B.; Lathuilière, B.; Ferry, S. Correlation of reefal Oxfordian episodes and climatic implications in the eastern Paris Basin (France). *Terra Nova* **2006**, *18*, 191–201. [CrossRef]
16. Ferry, S.; Pellenard, P.; Collin, P.Y.; Thierry, J.; Marchand, D.; Deconinck, J.F.; Robin, C.; Carpentier, C.; Durlet, C.; Curial, A. Synthesis of recent stratigraphic data on Bathonian to Oxfordian deposits of the eastern Paris Basin. *Mémoire Société Géologique Fr.* **2007**, *178*, 37–57.
17. Xiong, Q.; Yang, D.; Chen, W. Multi-scale modelling of gas flow in nanoscale pore space with fractures. *J. Rock Mech. Geotech. Eng.* **2020**, *12*, 32–40. [CrossRef]
18. Zhang, C.; Rothfuchs, T. Experimental study of the hydro-mechanical behaviour of the Callovo-Oxfordian argillite. *Appl. Clay Sci.* **2004**, *26*, 325–336. [CrossRef]
19. Esteban, L.; Bouchez, J.L.; Trouiller, A. The Callovo-Oxfordian argillites from the eastern Paris Basin: Magnetic data and petrofabrics. *Comptes Rendus Geosci.* **2006**, *338*, 867–881. [CrossRef]
20. Pellenard, P.; Deconinck, J.-F. Mineralogical variability of Callovo-Oxfordian clays from the Paris Basin and the Subalpine Basin. *Comptes Rendus Geosci.* **2006**, *338*, 854–866. [CrossRef]
21. Pellenard, P.; Deconinck, J.-F.; Marchand, D.; Thierry, J.; Fortwengler, D.; Vigneron, G. Contrôle géodynamique de la sédimentation argileuse du Callovien-Oxfordien moyen dans l'Est du bassin de Paris: Influence eustatique et volcanique. *Comptes Rendus L'académie Sci.-Ser. IIA-Earth Planet. Sci.* **1999**, *328*, 807–813. [CrossRef]
22. Collin, P.Y.; Elion, P.; Thierry, J.; Marchand, D.; Pellenard, P.; Trouiller, A. Le Callovo-Oxfordien de l'Est du bassin de Paris: Biochronologie, corrélations et évolution sédimentaire. Apports des travaux de l'ANDRA. *Trav. Doc. Lab. Géologie Lyon* **2002**, *156*, 79–80.
23. Yven, B.; Sammartino, S.; Geraud, Y.; Homand, F.; Villieras, F. Mineralogy, texture and porosity of Callovo-Oxfordian argillites of the Meuse/Haute-Marne region (eastern Paris Basin). *Mémoires Société Géologique Fr.* **2007**, *178*, 73–90.
24. Descostes, M.; Blin, V.; Bazer-Bachi, F.; Meier, P.; Grenut, B.; Radwan, J.; Schlegel, M.; Buschaert, S.; Coelho, D.; Tevissen, E. Diffusion of anionic species in Callovo-Oxfordian argillites and Oxfordian limestones (Meuse/Haute–Marne, France). *Appl. Geochem.* **2008**, *23*, 655–677. [CrossRef]
25. Sammartino, S.; Bouchet, A.; Prêt, D.; Parneix, J.-C.; Tevissen, E. Spatial distribution of porosity and minerals in clay rocks from the Callovo-Oxfordian formation (Meuse/Haute-Marne, Eastern France)—Implications on ionic species diffusion and rock sorption capability. *Appl. Clay Sci.* **2003**, *23*, 157–166. [CrossRef]
26. Boulin, P.F.; Angulo-Jaramillo, R.; Daian, J.-F.; Talandier, J.; Berne, P. Pore gas connectivity analysis in Callovo-Oxfordian argillite. *Appl. Clay Sci.* **2008**, *42*, 276–283. [CrossRef]
27. Clauer, N.; Fourcade, S.; Cathelineau, M.; Girard, J.P.; Vincent, B.; Elie, M.; Buschaert, S.; Rousset, D. A review of studies on the diagenetic evolution of the Dogger-to-Tithonian sedimentary sequence in the eastern Paris Basin-Impact on the physical and chemical rock properties: A multi-disciplinary approach to the eastern jurassic border of the Paris basin (Meuse/ Haute Marne). *Mém. Soc. Géol. Fr.* **2007**, *178*, 59–71.
28. Vincent, B.; Brigaud, B.; Emmanuel, L.; Loreau, J.P. High resolution ion microprobe investigation of the δ18O of carbonate cements (Jurassic, Paris Basin, France): New insights and pending questions. *Sediment. Geol.* **2017**, *350*, 42–54. [CrossRef]
29. Vincent, B.; Rambeau, C.; Emmanuel, L.; Loreau, J.-P. Sedimentology and trace element geochemistry of shallow-marine carbonates: An approach to paleoenvironmental analysis along the Pagny-sur-Meuse Section (Upper Jurassic, France). *Facies* **2006**, *52*, 69–84. [CrossRef]
30. Guillocheau, F.; Robin, C.; Allemand, P.; Bourquin, S.; Brault, N.; Dromart, G.; Friedenberg, R.; Garcia, J.-P.; Gaulier, J.-M.; Gaumet, F.; et al. Meso-Cenozoic geodynamic evolution of the Paris Basin: 3D stratigraphic constraints. *Geodin. Acta* **2000**, *13*, 189–245. [CrossRef]
31. Robin, C.; Guillocheau, F.; Allemand, P.; Bourquin, S.; Dromart, G.; Gaulier, J.-M.; Prijac, C. Echelles de temps et d'espace du controle tectonique d'un bassin flexural intracratonique; le bassin de Paris. *BSGF—Earth Sci. Bull.* **2000**, *171*, 181–196. [CrossRef]
32. Lacombe, O.; Obert, D. Héritage structural et déformation de couverture: Plissement et fracturation tertiaires dans l'Ouest du bassin de Paris. *Comptes Rendus L'académie Sci.-Ser. IIA-Earth Planet. Sci.* **2000**, *330*, 793–798. [CrossRef]
33. Beccaletto, L.; Hanot, F.; Serrano, O.; Marc, S. Overview of the subsurface structural pattern of the Paris Basin (France): Insights from the reprocessing and interpretation of regional seismic lines. *Mar. Pet. Geol.* **2011**, *28*, 861–879. [CrossRef]

34. Rocher, M.; Cushing, M.; Lemeille, F.; Lozac'H, Y.; Angelier, J. Intraplate paleostresses reconstructed with calcite twinning and faulting: Improved method and application to the eastern Paris Basin (Lorraine, France). *Tectonophysics* **2004**, *387*, 1–21. [CrossRef]
35. Beccaletto, L.; Capar, L.; Serrano, O.; Marc, S. Structural evolution and sedimentary record of the Stephano-Permian basins occurring beneath the Mesozoic sedimentary cover in the southwestern Paris basin (France). *BSGF—Earth Sci. Bull.* **2015**, *186*, 429–450. [CrossRef]
36. Ziegler, P. Collision related intra-plate compression deformations in Western and Central Europe. *J. Geodyn.* **1990**, *11*, 357–388. [CrossRef]
37. Ziegler, P.A. European Cenozoic rift system. *Tectonophysics* **1992**, *208*, 91–111. [CrossRef]
38. Dercourt, J. *Atlas Peri-Tethys, Palaeogeographical Maps, 24 Maps and Explanatory Notes*; CCGM/CGMW: Paris, France, 2000.
39. Blakey, R. Deep Time Maps. 2017. Available online: http://deeptimemaps.com (accessed on 7 October 2021).
40. Carpentier, C. Géométries et Environnements de Dépôt de l'Oxfordien de l'Est du Bassin de Paris. Ph.D. Thesis, Université de Nancy 1, Nancy, France, 2004.
41. Vincent, B. Sedimentology and Geochemistry of Carbonates Diagenesis. Application to the Malm of the Eastern Edge of the Paris Basin. Ph.D. Thesis, Université de Bourgogne, Dijon, France, 2001.
42. Vincent, B.; Emmanuel, L.; Houel, P.; Loreau, J.-P. Geodynamic control on carbonate diagenesis: Petrographic and isotopic investigation of the Upper Jurassic formations of the Paris Basin (France). *Sediment. Geol.* **2007**, *197*, 267–289. [CrossRef]
43. Haq, B.U.; Hardenbol, J.; Vail, P.R. Chronology of Fluctuating Sea Levels Since the Triassic. *Science* **1987**, *235*, 1156–1167. [CrossRef]
44. Hardenbol, J.; Thierry, J.; Farley, M.B.; Jacquin, T.; de Graciansky, P.-C.; Vail, P.R. Mesozoic and Cenozoic Sequence Chronostratigraphic Framework of European Basins. *SEPM Soc. Sediment. Geol. Spec. Publ.* **1999**, *60*, 3–13. [CrossRef]
45. Dera, G.; Brigaud, B.; Monna, F.; Laffont, R.; Pucéat, E.; Deconinck, J.-F.; Pellenard, P.; Joachimski, M.; Durlet, C. Climatic ups and downs in a disturbed Jurassic world. *Geology* **2011**, *39*, 215–218. [CrossRef]
46. Cecca, F.; Garin, B.M.; Marchand, D.; Lathuiliere, B.; Bartolini, A. Paleoclimatic control of biogeographic and sedimentary events in Tethyan and peri-Tethyan areas during the Oxfordian (Late Jurassic). *Palaeogeogr. Palaeoclim. Palaeoecol.* **2005**, *222*, 10–32. [CrossRef]
47. Brigaud, B.; Pucéat, E.; Pellenard, P.; Vincent, B.; Joachimski, M.M. Climatic fluctuations and seasonality during the Late Jurassic (Oxfordian–Early Kimmeridgian) inferred from δ18O of Paris Basin oyster shells. *Earth Planet. Sci. Lett.* **2008**, *273*, 58–67. [CrossRef]
48. Pellenard, P.; Tramoy, R.; Pucéat, E.; Huret, E.; Martinez, M.; Bruneau, L.; Thierry, J. Carbon cycle and sea-water palaeotemperature evolution at the Middle–Late Jurassic transition, eastern Paris Basin (France). *Mar. Pet. Geol.* **2014**, *53*, 30–43. [CrossRef]
49. Dromart, G.; Garcia, J.-P.; Gaumet, F.; Picard, S.; Rousseau, M.; Atrops, F.; Lécuyer, C.; Sheppard, S.M.F. Perturbation of the carbon cycle at the Middle/Late Jurassic transition: Geological and geochemical evidence. *Am. J. Sci.* **2003**, *303*, 667–707. [CrossRef]
50. Carmeille, M.; Bourillot, R.; Pellenard, P.; Dupias, V.; Schnyder, J.; Riquier, L.; Mathieu, O.; Brunet, M.-F.; Enay, R.; Grossi, V.; et al. Formation of microbial organic carbonates during the Late Jurassic from the Northern Tethys (Amu Darya Basin, Uzbekistan): Implications for Jurassic anoxic events. *Glob. Planet. Chang.* **2020**, *186*, 103127. [CrossRef]
51. Li, G.; Xia, G.; Yi, H.; Wu, C.; Wagreich, M. Climate changes as recorded in stable carbon isotopic compositions of the Late Jurassic marine sedimentary succession in the Qiangtang Basin, Northern Tibet. *J. Southeast Asian Earth Sci.* **2022**, *236*, 105317. [CrossRef]
52. Rais, P.; Louis-Schmid, B.; Bernasconi, S.M.; Weissert, H. Palaeoceanographic and palaeoclimatic reorganization around the Middle–Late Jurassic transition. *Palaeogeogr. Palaeoclim. Palaeoecol.* **2007**, *251*, 527–546. [CrossRef]
53. Louis-Schmid, B.; Rais, P.; Bernasconi, S.M.; Pellenard, P.; Collin, P.Y.; Weissert, H. Detailed record of the mid-Oxfordian (Late Jurassic) positive carbon-isotope excursion in two hemipelagic sections (France and Switzerland): A plate tectonic trigger? *Palaeogeogr. Palaeoclimatol. Palaeoecol.* **2007**, *248*, 459–472. [CrossRef]
54. Louis-Schmid, B.; Rais, P.; Schaeffer, P.; Bernasconi, S.M.; Weissert, H. Plate tectonic trigger of changes in pCO2 and climate in the Oxfordian (Late Jurassic): Carbon isotope and modeling evidence. *Earth Planet. Sci. Lett.* **2007**, *258*, 44–60. [CrossRef]
55. Wierzbowski, H. Detailed oxygen and carbon isotope stratigraphy of the Oxfordian in Central Poland. *Geol. Rundsch.* **2002**, *91*, 304–314. [CrossRef]
56. Wierzbowski, H. Carbon and oxygen isotope composition of Oxfordian–Early Kimmeridgian belemnite rostra: Palaeoenvironmental implications for Late Jurassic seas. *Palaeogeogr. Palaeoclim. Palaeoecol.* **2004**, *203*, 153–168. [CrossRef]
57. Wierzbowski, H.; Dembicz, K.; Praszkier, T. Oxygen and carbon isotope composition of Callovian–Lower Oxfordian (Middle–Upper Jurassic) belemnite rostra from central Poland: A record of a Late Callovian global sea-level rise? *Palaeogeogr. Palaeoclimatol. Palaeoecol.* **2009**, *283*, 182–194. [CrossRef]
58. Wierzbowski, H.; Rogov, M.A.; Matyja, B.A.; Kiselev, D.; Ippolitov, A. Middle–Upper Jurassic (Upper Callovian–Lower Kimmeridgian) stable isotope and elemental records of the Russian Platform: Indices of oceanographic and climatic changes. *Glob. Planet. Chang.* **2013**, *107*, 196–212. [CrossRef]
59. Thierry, J.; Marchand, D.; Fortwengler, D. Détermination des ammonites du CallovieneOxfordien (Jurassique moyen-supérieur) et calibrage biochronostratigraphique des unités lithologiques traversées par les forages Andra 2007–2008. Rapport ANDRA C.RP.0UNB.10.0001. *Synthèse Bio-Chronostratigraphique Zone Transposition* **2010**, 163.
60. Enay, R.; Boullier, A. L'âge du complexe récifal des côtes de meuse entre verdun et commercy et la stratigraphie de l'oxfordien dans l'est du bassin de Paris. *Geobios* **1981**, *14*, 727–771. [CrossRef]

61. Pellenard, P.; Deconinck, J.-F.; Huff, W.D.; Thierry, J.; Marchand, D.; Fortwengler, D.; Trouiller, A. Characterization and correlation of Upper Jurassic (Oxfordian) bentonite deposits in the Paris Basin and the Subalpine Basin, France. *Sedimentology* **2003**, *50*, 1035–1060. [CrossRef]
62. Dunham, R.J. Classification of carbonate rocks according to depositional textures. *AAPG Mem.* **1962**, *1*, 108–121.
63. Embry, A.F.; Klovan, J.E. A late Devonian reef tract on northeastern Banks Island, NWT. *Bull. Can. Pet. Geol.* **1971**, *19*, 730–781.
64. Taylor, A.M.; Goldring, R. Description and analysis of bioturbation and ichnofabric. *J. Geol. Soc.* **1993**, *150*, 141–148. [CrossRef]
65. Walther, J. *Einleitung in Die Geologie Als Historische Wissenschaft: Beobachtungen über Die Bildung der Gesteine und Ihrer Organischen Einschlüsse*; G. Fischer Verlag: Jena, Germany, 1894; Volume 3, pp. 535–1055.
66. Middleton, G.V. Johannes Walther's law of the correlation of facies. *Geol. Soc. Am. Bull.* **1973**, *84*, 979–988. [CrossRef]
67. Burchette, T.; Wright, V. Carbonate ramp depositional systems. *Sediment. Geol.* **1992**, *79*, 3–57. [CrossRef]
68. Vail, P.R.; Colin, J.P.; Jan du Chene, R.; Kuchly, J.; Mediavilla, F.; Trifilieff, V. La stratigraphie séquentielle et son application aux corrélations chronostratigrahiques dans le Jurassique du bassin de Paris. *Bull. Société Géologique Fr.* **1987**, *8*, 1301–1321. [CrossRef]
69. Van Wagoner, J.C.; Posamentier, H.W.; Mitchum, R.M.; Vail, P.R.; Sarg, J.F.; Loutit, T.S.; Hardenbol, J. An overview of the fundamentals of sequence stratigraphy and key definitions. In *Sea Level Changes–An Integrated Approach*; Wilgus, C.K., Hastings, B.S., St. C. Kendall, C.G., Posamentier, H.W., Ross, C.A., Van Wagoner, J.C., Eds.; SEPM: Tulsa, OK, USA, 1988; Volume 42, pp. 39–45. [CrossRef]
70. Thierry, J.; Marchand, D.; Fortwengler, D.; Bonnot, A.; Jardat, R. Les ammonites du Callovien–Oxfordien des sondages Andra dans l'Est du bassin de Paris: Synthèse biochronostratigraphique, intérêts paléoécologique et paléobiogéographique. *Comptes Rendus Geosci.* **2006**, *338*, 834–853. [CrossRef]
71. Packard, J.; Reimer, J.; Schink, A.; Hewitt, M.; Hamilton, D.; Marshall, M.; Arts, A.; Evers, S.N.; Embry, A.; Middleton, D.; et al. Canadian society of petroleum geologists 2004/2005 report of activities. *Bull. Can. Pet. Geol.* **2005**, 1–53. [CrossRef]
72. MacEachern, J.A.; Pemberton, S.G.; Gingras, M.K.; Bann, K.L.; Dafoe, L.T. Uses of Trace Fossils in Genetic Stratigraphy. In *Trace Fossils*; Elsevier: Amsterdam, The Netherlands, 2007; pp. 110–134. [CrossRef]
73. Chiarella, D.; Longhitano, S.G.; Tropeano, M. Types of mixing and heterogeneities in siliciclastic-carbonate sediments. *Mar. Pet. Geol.* **2017**, *88*, 617–627. [CrossRef]
74. Lokier, S.W.; Al Junaibi, M. The petrographic description of carbonate facies: Are we all speaking the same language? *Sedimentology* **2016**, *63*, 1843–1885. [CrossRef]
75. Seilacher, A. *Trace Fossil Analysis*; Springer Science & Business Media: Tübingen, Germany, 2007.
76. Myrow, P.M.; Southard, J.B. Tempestite deposition. *J. Sediment. Res.* **1996**, *66*, 875–887.
77. Dumas, S.; Arnott, R.; Southard, J.B. Experiments on Oscillatory-Flow and Combined-Flow Bed Forms: Implications for Interpreting Parts of the Shallow-Marine Sedimentary Record. *J. Sediment. Res.* **2005**, *75*, 501–513. [CrossRef]
78. Knaust, D. The ichnogenus Rhizocorallium: Classification, trace makers, palaeoenvironments and evolution. *Earth-Sci. Rev.* **2013**, *126*, 1–47. [CrossRef]
79. Harms, J.C.; Southard, J.B.; Spearing, D.R.; Walker, R.G. *Depositional Environments as Interpreted from Primary Sedimentary Structures and Stratification Sequences*; SEPM: Tulsa, OK, USA, 1975.
80. Ito, M.; Ishigaki, A.; Nishikawa, T.; Saito, T. Temporal variation in the wavelength of hummocky cross-stratification: Implications for storm intensity through Mesozoic and Cenozoic. *Geology* **2001**, *29*, 87–89. [CrossRef]
81. Immenhauser, A. Estimating palaeo-water depth from the physical rock record. *Earth-Sci. Rev.* **2009**, *96*, 107–139. [CrossRef]
82. Coffey, B.P.; Read, J.F. Mixed carbonate–siliciclastic sequence stratigraphy of a Paleogene transition zone continental shelf, southeastern USA. *Sediment. Geol.* **2004**, *166*, 21–57. [CrossRef]
83. Zecchin, M.; Catuneanu, O. High-resolution sequence stratigraphy of clastic shelves VI: Mixed siliciclastic-carbonate systems. *Mar. Pet. Geol.* **2017**, *88*, 712–723. [CrossRef]
84. Haq, B.U. Jurassic Sea-Level Variations: A Reappraisal. *GSA Today* **2017**, *28*, 4–10. [CrossRef]
85. Hesselbo, S.; Ogg, J.; Ruhl, M.; Hinnov, L.; Huang, C. *The Jurassic Period, in Geologic Time Scale 2020*; Elsevier: Amsterdam, The Netherlands, 2020; pp. 955–1021.
86. Gygi, R.A.; Coe, A.L.; Vail, P.R.; de Graciansky, P.-C.; Hardenbol, J.; Jacquin, T. Sequence Stratigraphy of the Oxfordian and Kimmeridgian Stages (Late Jurassic) in Northern Switzerland. In *Mesozoic and Cenozoic Sequence Stratigraphy of European Basins*; de Graciansky, P.C., Hardenbol, J., Jacquin, T., Vail, P.R., Eds.; Special Publications of SEPM: Tulsa, OK, USA, 1999; Volume 60, pp. 527–544. [CrossRef]
87. Ramajo, J.; Aurell, M. Long-term Callovian–Oxfordian sea-level changes and sedimentation in the Iberian carbonate platform (Jurassic, Spain): Possible eustatic implications. *Basin Res.* **2008**, *20*, 163–184. [CrossRef]
88. Collin, P.-Y. Environnements, Géochimie et Processus de Formation de Séries Condensées au Callovo-Oxfordien: Du Bassin de Paris à des Considérations Globales. Ph.D. Thesis, Université de Bourgogne, Dijon, France, 2000.
89. Read, J.F. Carbonate Platform Facies Models. *Am. Assoc. Pet. Geol. Bull.* **1985**, *69*, 1–21.
90. Pomar, L. Types of carbonate platforms: A genetic approach. *Basin Res.* **2001**, *13*, 313–334. [CrossRef]
91. Calvet, F.M.T.; Tucker, M.E.; Henton, J. Middle Triassic carbonate ramp systems in the Catalan Basin, northeast Spain: Facies, systems tracts, sequences and controls. *Spec. Publs. Int. Ass. Sediment.* **1990**, *9*, 79–108.
92. Lathuilière, B.; Gaillard, C.; Habrant, N.; Bodeur, Y.; Boullier, A.; Enay, R.; Hanzo, M.; Marchand, D.; Thierry, J.; Werner, W. Coral zonation of an Oxfordian reef tract in the northern French Jura. *Facies* **2005**, *50*, 545–559. [CrossRef]

93. Martin-Garin, B.; Lathuilière, B.; Geister, J. The shifting biogeography of reef corals during the Oxfordian (Late Jurassic). A climatic control? *Palaeogeogr. Palaeoclim. Palaeoecol.* **2012**, *365–366*, 136–153. [CrossRef]
94. James, N.P. The cool-water carbonate depositional realm. In *Cool-Water Carbonates*; James, N.P., Clarke, N.P., Eds.; Special Publications of SEPM: Tulsa, OK, USA, 1997. [CrossRef]
95. Föllmi, K.B.; Godet, A.; Bodin, S.; Linder, P. Interactions between environmental change and shallow water carbonate buildup along the northern Tethyan margin and their impact on the Early Cretaceous carbon isotope record. *Paleoceanography* **2006**, *21*, 1–16. [CrossRef]
96. Michel, J.; Borgomano, J.; Reijmer, J.J. Heterozoan carbonates: When, where and why? A synthesis on parameters controlling carbonate production and occurrences. *Earth-Sci. Rev.* **2018**, *182*, 50–67. [CrossRef]
97. Schlöder, C.; D'Croz, L. Responses of massive and branching coral species to the combined effects of water temperature and nitrate enrichment. *J. Exp. Mar. Biol. Ecol.* **2004**, *313*, 255–268. [CrossRef]
98. Hennige, S.; Smith, D.; Perkins, R.; Consalvey, M.; Paterson, D.; Suggett, D.J. Photoacclimation, growth and distribution of massive coral species in clear and turbid waters. *Mar. Ecol. Prog. Ser.* **2008**, *369*, 77–88. [CrossRef]
99. Gygi, R.A. *Integrated Stratigraphy of the Oxfordian and Kimmeridgian (Late Jurassic) in Northern Switzerland and Adjacent Southern Germany*; Birkhäuser: Basel, Switzerland, 2000. [CrossRef]
100. Baria, L.R.; Stoudt, D.L.; Harris, P.M.; Crevello, P.D. Upper Jurassic reefs of Smackover formation, United States gulf coast. *AAPG Bull.* **1982**, *66*, 1449–1482.
101. Hautevelle, Y.; Michels, R.; Malartre, F.; Trouiller, A. Vascular plant biomarkers as proxies for palaeoflora and palaeoclimatic changes at the Dogger/Malm transition of the Paris Basin (France). *Org. Geochem.* **2006**, *37*, 610–625. [CrossRef]
102. Strasser, A.; Pittet, B.; Hillgärtner, H.; Pasquier, J.-B. Depositional sequences in shallow carbonate-dominated sedimentary systems: Concepts for a high-resolution analysis. *Sediment. Geol.* **1999**, *128*, 201–221. [CrossRef]
103. Plint, A.G. Control of sea level change. *Facies Models Response Sea Level Change* **1992**, 15–25.
104. Pittet, B. Contrôles climatiques, eustatiques et tectoniques sur des systèmes mixtes carbonates-siliciclastiques de plate-forme: Exemples de l'Oxfordien (Jura suisse, Normandie, Espagne). Ph.D. Thesis, University of Fribourg, Fribourg, Switzerland, 1996.
105. Shackleton, N. Oxygen isotopes, ice volume and sea level. *Quat. Sci. Rev.* **1987**, *6*, 183–190. [CrossRef]
106. Gornitz, V.; Lebedeff, S.; Hansen, J. Global Sea Level Trend in the Past Century. *Science* **1982**, *215*, 1611–1614. [CrossRef]
107. Schulz, M.; Schäfer-Neth, C. Translating Milankovitch climate forcing into eustatic fluctuations via thermal deep water expansion: A conceptual link. *Terra Nova* **1997**, *9*, 228–231. [CrossRef]
108. Jacobs, D.K.; Sahagian, D.L. Climate-induced fluctuations in sea level during non-glacial times. *Nature* **1993**, *361*, 710–712. [CrossRef]
109. Donnadieu, Y.; Dromart, G.; Goddéris, Y.; Pucéat, E.; Brigaud, B.; Dera, G.; Dumas, C.; Olivier, N. A mechanism for brief glacial episodes in the Mesozoic greenhouse. *Paleoceanography* **2011**, *26*, 1–10. [CrossRef]
110. Frakes, L.A.; Francis, J.E.; Syktus, J.I. *Climate Modes of the Phanerozoic*; Cambridge University Press: Cambridge, UK, 1992. [CrossRef]
111. Mutterlose, J.; Ruffell, A. Milankovitch-scale palaeoclimate changes in pale–dark bedding rhythms from the Early Cretaceous (Hauterivian and Barremian) of eastern England and northern Germany. *Palaeogeogr. Palaeoclim. Palaeoecol.* **1999**, *154*, 133–160. [CrossRef]
112. Föllmi, K. Early Cretaceous life, climate and anoxia. *Cretac. Res.* **2011**, *35*, 230–257. [CrossRef]
113. Wendler, J.E.; Wendler, I. What drove sea-level fluctuations during the mid-Cretaceous greenhouse climate? *Palaeogeogr. Palaeoclimatol. Palaeoecol.* **2016**, *441*, 412–419. [CrossRef]
114. Hay, W.W.; Leslie, M.A. Could possible changes in global groundwater reservoir cause eustatic sea-level fluctuations. *Sea-Level Chang.* **1990**, 161–170.
115. Sames, B.; Wagreich, M.; Conrad, C.P.; Iqbal, S. Aquifer-eustasy as the main driver of short-term sea-level fluctuations during Cretaceous hothouse climate phases. *Geol. Soc. London Spéc. Publ.* **2019**, *498*, 9–38. [CrossRef]
116. Martinez, M.; Dera, G. Orbital pacing of carbon fluxes by a ∼9-My eccentricity cycle during the Mesozoic. *Proc. Natl. Acad. Sci. USA* **2015**, *112*, 12604–12609. [CrossRef]